# “The Nature of Water in the Voltage-gated Hv1 Proton Channel from *Ciona intestinalis* and its potential role in proton permeation”

**Tesis entregada a**
**UNIVERSIDAD DE VALPARAÍSO**

**En Cumplimiento Parcial de los requisitos para optar al grado de Doctor en Ciencias con Mención en Biofísica y Biología Computacional**

**Facultad de Ciencias**

**Por**

**Juan José Alvear Arias**

**2023**

**Dirigida por:**
**Dr. Carlos González León**
**Dr. José Antonio Gárate Chateau**

# FACULTAD DE CIENCIAS,
# UNIVERSIDAD DE VALPARAÍSO

# INFORME DE APROBACIÓN DE TESIS DE DOCTORADO

Se informa a la Facultad de Ciencias que la Tesis de Doctorado presentada por:
JUAN JOSÉ ALVEAR ARIAS

Ha sido aprobada por la comisión de la Evaluación de la tesis como requisito para optar al grado de Doctor en Ciencias con mención en Biofísica y Biología Computacional, en el examen de Defensa de Tesis rendido el día 28 del mes de Julio 2023.

**Director de Tesis:**

Dr. Carlos González León
**…….**

**Codirector de Tesis:**

Dr. José Antonio Garate Chateau
**…….**

**Comisión de Evaluación de la Tesis**

*Evaluador y Presidente de la comisión:*
Dr. Alan Neely
**…….**

*Evaluador:*
Dr. Juan Carlos Sáez
**…….**

*Evaluador externo al claustro del programa:*
Dr. Marcelo Ozu
**…….**

*Esta página ha sido intencionalmente dejada en blanco*

# Index

# Resumen

A la fecha el mecanismo de permeación del canal de protones sensible a voltaje, Hv1, es materia de controversia. Esto es debido a que no existe la resolución de una estructura abierta de la proteína. Actualmente hay dos mecanismos que intentan explicar el mecanismo de permeación de Hv1. El primero propone que la conducción de protones ocurre de una manera similar al mecanismo de Grotthuss, estableciéndose un continuo de agua cuando la proteína se encuentra abierta, lo que permite el salto de protones a través de los puentes de hidrógenos que se establecen entre las moléculas de agua. El otro modelo, en cambio, propone que el continuo de agua es interrumpido entre la interacción del filtro de selectividad y la segunda y/o tercera arginina del sensor de potencial. A pesar de esto, ninguno de los dos modelos satisface la evidencia experimental, ya que hay gran cantidad de datos que sugieren que la asparagina altamente conservada de la alfa hélice S4 (N264 en CiHv1) es importante en el mecanismo de conducción. Los modelos en discusión no contemplan un papel para este residuo en el mecanismo de conducción. Dado que el mecanismo de conducción de protones y la naturaleza del agua dentro de la proteína son elementos que no pueden ser separados, en este trabajo a través de mediciones electrofisiológicas, dinámica molecular y mediciones de cambios de volumen en ovocitos de *X. laevis*, observamos que las mutaciones dirigidas a la asparagina de la alfa hélice S4 en el canal Hv1 de *C. intestinalis* afectan las propiedades de conducción y que dicho cambio en las propiedades conductivas está fuertemente relacionado con las características de hidratación del canal, como también de la configuración de los ángulos de dipolo de las moléculas de agua en la zona de constricción del canal. Por otro lado, se observó que en ovocitos inyectados con Hv1 poseían un mayor coeficiente de permeabilidad de agua, sugiriendo que la proteína permite el movimiento de agua. Toda la evidencia en conjunto permite proponer un modelo de conducción de protones el cual posee dos elementos críticos: (1) la configuración de las moléculas de agua en la zona de constricción del canal, además de una zona permanentemente hidratada que permite el paso de protones y, (2) el perfil electrostático en la vecindad de la zona

de constricción.


## Abstract

To date, the permeation mechanism of the voltage-gated proton (Hv1) channel is a matter of controversy. This is because there is no resolution of an open structure of the protein. Currently, there are two hypotheses that attempt to explain the Hv1 proton permeation mechanisms. The first proposes that proton conduction occurs in a *Grotthuss*-like mechanism, establishing a continuous flow of water when the protein is open, which allows protons to jump through hydrogen bonds established between water molecules. The other model, on the other hand, proposes that the continuous flow water is interrupted between the selectivity filter interaction and the second and/or third arginine of the potential sensor. Despite this, neither of the two models satisfies the evidence, as there is a large amount of data suggesting that the highly conserved asparagine of the S4 alpha helix is important in the conduction mechanism. The models under discussion do not consider a role for this residue in the conduction mechanism. Since the proton conduction mechanism and the nature of water molecules within the protein are elements that cannot be separated, in this work through electrophysiological measurements, molecular dynamics, and volume change measurements in *X. laevis* oocytes, we observed that mutations directed to the asparagine of the S4 alpha helix in Hv1 channel of *C. intestinalis* affect the conductive properties and that such changes in conductive properties are strongly related to the hydration characteristics of the channel, as well as the dipole angle configurations of the water molecules in the channel constriction zone. On the other hand, it was observed that oocytes injected with Hv1 had higher permeability coefficients, suggesting that the protein allows water movement. All the evidence together allows us to propose a proton conduction model which has two critical elements: (1) the configuration of water molecules in the channel constriction zone, in addition to a permanently hydrated zone that allows proton passage, and (2) the electrostatic profile at the vicinity of the constriction zone.

# Introduction

## 1) Water and its Interactions with Biomolecules: The Biology Framework

*"I believe that, with the progressive application of the methods of structural chemistry to physiological problems, we will see that the importance of hydrogen bonding in physiology is greater than that of any other structural feature "*

*-Linus Pauling,*
*The Nature of the Chemical Bond, 1939*

In July 2018, researchers from the Mars Express mission of the European Space Agency (ESA) announced the detection of a subterranean lake on Mars. The mass of water found on the red planet was characterized as being rich in salts, which is key to keeping it in a liquid state. This interesting discovery could help answer the big question: Is there life on Mars? (Article "In search of Water on Mars", National Geographic, August 2022).

When we think of life, we immediately think of water. Water is the most abundant substance in biological systems and constitutes around 70% of their weight in most cases. According to the hypothesis, the first living organisms arose in an aquatic environment and the course of evolution was directed towards life with its diversity of identities and characteristics based on the qualities of this aquatic milieu. Thus, biochemical reactions and molecular mechanisms that sustain life mainly occur in aqueous solution, as the structural and functional characteristics of biomolecules adapt to the physicochemical characteristics of water (Brini et al. 2017). For this reason, to rigorously approach certain molecular mechanisms, it is crucial to understand the interactions that water molecules have with biomolecules.

Water is an acceptor and donor molecule of hydrogen bonds (hereafter, H-bonds). H-bonds between $H_2O$-$H_2O$ provide the attractive forces that confer unique properties, such as being liquid at room temperature, solid and crystalline at low

temperatures, and with higher melting and boiling points compared to other common solvents.

H-bonds are not exclusively between water molecules. They can easily form between electronegative atoms from functional groups such as alcohols, aldehydes, ketones, and nitrogenous compounds. In the case of amino acids, these can be related through H-bonds with their N- and C-terminal. Additionally, the polar amino acids side chains can form H-bonds, while the charged positive or negative amino acid side chains can form salt bridges (which we will abbreviate as S-bridges) **(Figure 1)**.

These types of interactions have an important effect on the structure, stability, dynamics, and function of proteins (Levy and Onuchic 2004). In fact, networks of $H_2O$ linked by H-bonds form connections between solutes that allow larger molecules (such as protein and nucleic acids) to interact with each other over distances of several nanometers without physical contact.

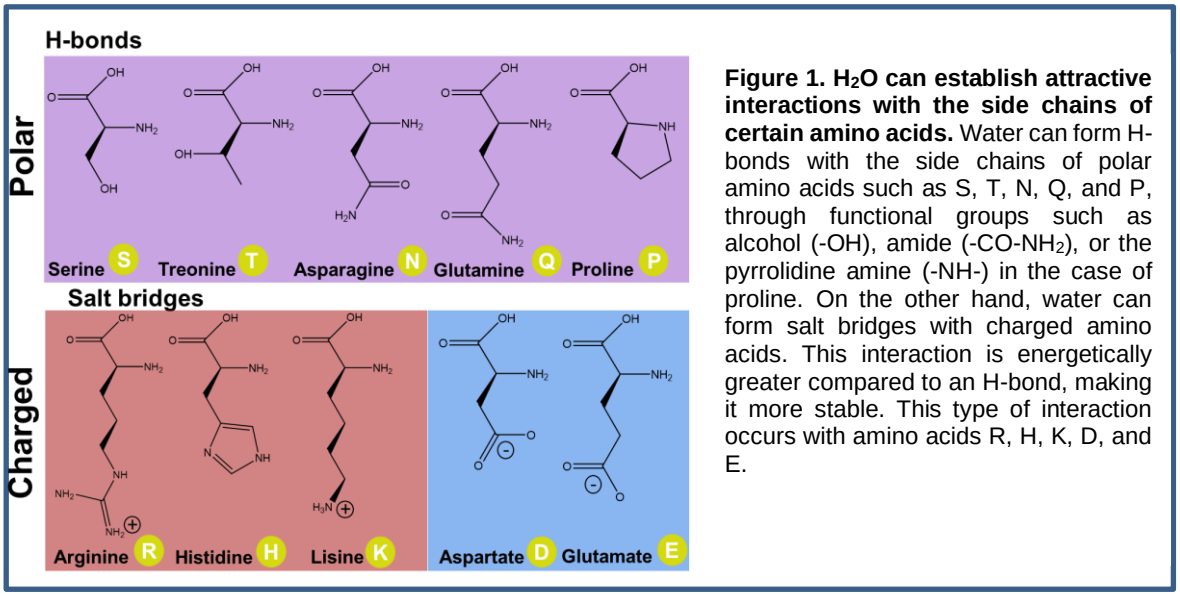


**Figure 1. $H_2O$ can establish attractive interactions with the side chains of certain amino acids.** Water can form H-bonds with the side chains of polar amino acids such as S, T, N, Q, and P, through functional groups such as alcohol (-OH), amide (-CO-$NH_2$), or the pyrrolidine amine (-NH-) in the case of proline. On the other hand, water can form salt bridges with charged amino acids. This interaction is energetically greater compared to an H-bond, making it more stable. This type of interaction occurs with amino acids R, H, K, D, and E.

Therefore, water not only interacts with the charged or polar surfaces of proteins, but it also becomes a structural component in interior cavities. Here, water molecules form stable clusters, which acquire different configurations (i.e., distribution and orientation of the dipole angle) depending on the characteristics of such a cavity

(Matthews and Liu 2009; Pérez et al. 2012; Rasaiah, Garde, and Hummer 2008; Yu et al. 1999).

Samples of these clusters have been reported in hydrophobic cavities of proteins. These water structures are stabilized due to repulsive forces of the hydrophobic cavities, promoting the interaction between structural water molecules (Matthews and Liu 2009). For example, interleukin 1β has four hydrophobic cavities that contain clusters of two or more water molecules with lifetimes of ~200 microseconds (Covalt et al. 2001). Directed mutations of critical residues that alter the interaction between water molecules and the cavity result in the structural destabilization of the protein (Covalt et al. 2001).

Thus, water has been included as an integral component in biomolecular systems for the last two decades, especially considering that interactions between water and proteins considerably improve structural predictions made with computational techniques such as Molecular Dynamics (MD) (Papoian et al. 2004).

## 2) Water and Proton Conduction

Water plays a fundamental role in proteins where proton conduction occurs. Water molecules have a slight tendency to reversibly ionize giving the equilibrium:

$$H_2O \leftrightarrow H^+ + OH^-$$

Although the dissociation of water is often shown as $H^+$, protons do not exist "naked" in aqueous solution, but rather are found forming covalent bonds with water, resulting in the structure known as the hydronium ion ($H_3O^+$) (Eigen 1964). The movement of protons in an electric field is extremely fast. Since protons move through the hydrogen bonds of water molecules in a sequence of proton-transfer reactions, and other ions diffuse between water molecules "dressing" their respective hydration boxes, proton diffusion in water is five times faster than ions such as $Na^+$, $K^+$ or $Cl^-$ (Agmon 1995; Buch-Pedersen et al. 2009). The model to explain the high mobility of protons in water is the *Grotthuss* mechanism, also known as proton hops model, postulated in 1805 by Theodor von Grotthuss, which proposes that proton transfer consists of rapid protonation-deprotonation reactions between neighboring water molecules along a H-bond wire (Agmon 1995; de Grotthuss 2006)[1] **(Figure 2A)**. In a water network, a proton that enters the cable will cause repulsion and consequently the propagation of the rest of the protons contained in the cable, so the proton that integrates into a cable is not the same as the one that comes out **(Figure 2B)** (Buch-Pedersen et al. 2009; Mathias and Marx 2007). It has been proposed that the rate-limiting step in proton motion is water reorientation between adjacent molecules to favor the proton transfer reaction (Agmon 1995). However, water is not a free rotor; rather, it is tightly coordinated by hydrogen bonding between four neighboring molecules in a structure that tends to be tetrahedral (Agmon 1995). Therefore, it has been proposed that this must be one of the most important elements to consider when explaining the proton mobility.

[1] The original article was printed in Rome in 1805 under the name "Mémorie sur la decomposition de l'eau et des corps qu'elle tient en dissolution á l'aide de l'electricité galvanique". The article cited in this document corresponds to the English translation which was made by Régis Pomés in 2006.

Additionally, at room temperature, the reorientation kinetics of water molecules takes about 1-2 ps, while proton hopping occurs in a similar magnitude of around 1.5 ps (Agmon 1995). This could potentially explain the rapid transportation rates of protons in aqueous solutions and consistently accounts for why the proton mobility in ice is one or two times faster than in liquid water (Eigen 1964).

Given the above, the study of $H^+$ transport cannot be separated from studies and observations of water within a system. Thus, it is not surprising that water clusters have been found in internal cavities of proteins specialized in proton transport. Some examples of this are the proton pump cytochrome C oxidase (Wikström, Verkhovsky, and Hummer 2003), bacteriorhodopsin (Bada Juarez et al. 2021; Garczarek et al. 2005; Mathias and Marx 2007; Schobert, Brown, and Lanyi 2003), and of course, the voltage-gated proton (Hv1) channel (Dudev et al. 2015; Morgan et al. 2013; Ramsey et al. 2010; Sakata et al. 2010a).

To understand how water may be modulating proton conduction in the Hv1 channel, we must first discuss the most important molecular determinants for channel conduction and its biophysical properties.

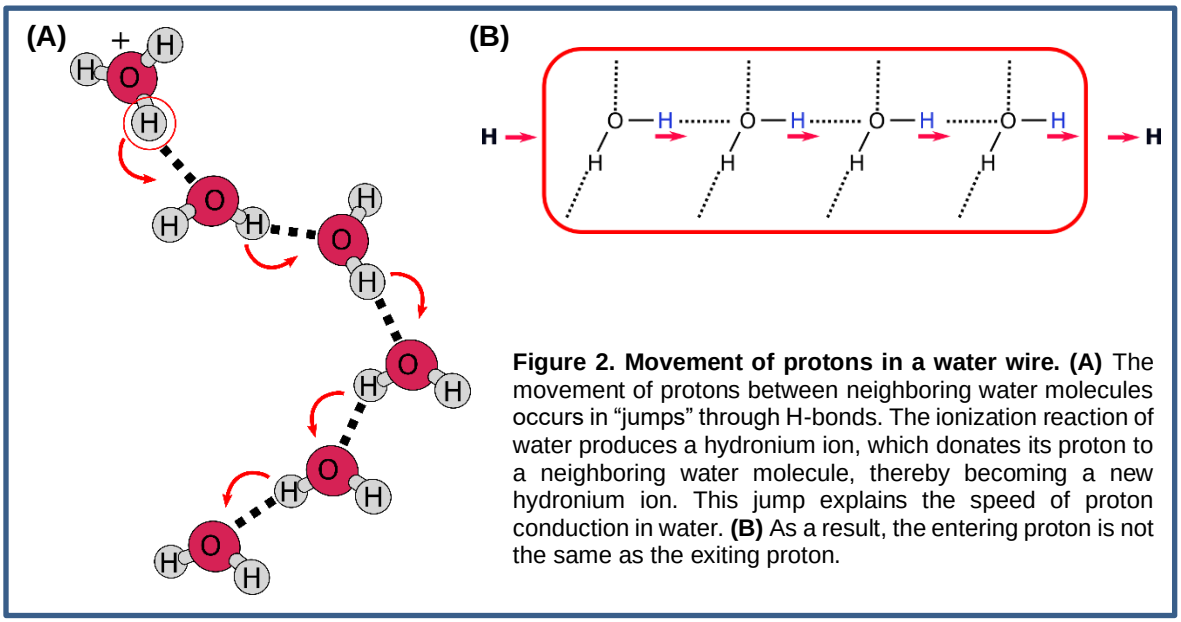


**Figure 2. Movement of protons in a water wire. (A)** The movement of protons between neighboring water molecules occurs in "jumps" through H-bonds. The ionization reaction of water produces a hydronium ion, which donates its proton to a neighboring water molecule, thereby becoming a new hydronium ion. This jump explains the speed of proton conduction in water. **(B)** As a result, the entering proton is not the same as the exiting proton.

## 3) Structural Characteristics and Biophysical Properties in the Conduction of the Hv1 Channel

The *hvcn1* gene encodes for the voltage-gated proton channel (Hv1), which is a transmembrane protein of ~30 kDa (Ramsey et al. 2006; Sasaki, et al. 2006). The architecture of this protein is characterized by four transmembrane alpha helices (S1-S4) with intracellular N- and C-terminal domains (Ramsey et al. 2006; Sasaki et al. 2006; Takeshita et al. 2014). It also features an alpha helix S0 located in the N-terminal region (between residues F88 to L95 in hHv1), which possibly plays a role in conferring structural stability and mediating membrane anchoring (Takeshita et al. 2014) **(Figure 3)**. The native oligomeric state of this protein corresponds to a homodimer, where both subunits of this channel interact through a coiled-coil type interaction between their C-terminals (Koch et al. 2008; Tombola et al. 2008). It is interesting that despite this protein is naturally forming dimers in biological systems, monomers can be obtained artificially by truncating the C- and part of the N-terminal. These monomers are fully functional and retain the properties of their dimeric counterpart because each subunit of the Hv1 channel contains all the functional domains of the protein, which are: voltage sensor, pH sensor, and proton permeation pathway. Next, I will discuss the characteristics and peculiarities of each of the functional domains, as well as some biophysical properties of the protein.

### I. The Voltage Sensor

The proton channel is a member of the large family of voltage-gated ion channels, specialized membrane proteins that detect changes in the electrical potential experienced by the cell membrane (Hille 2001). The ability to do this is primarily given because this family of proteins contains a voltage sensor in its structure, consisting of an array of positively charged residues (**+**) (usually R, K or H) generally contained in the S4 alpha helix, and these residues are arranged in the form of **+**xx**+**xx**+**xx**+**", *i.e.*, one charged residue every three positions (Bezanilla 2018). These charged residues are at the center of the membrane, so when the membrane potential suffers depolarization, the charged residues of this sensor undergo

electrostatic repulsion that induces a conformational change both in the transmembrane segments and in the protein in global terms (Bezanilla 2018). The conformational change causes the protein to transition from a non-conductive state to a conductive one.

In the case of the Hv1 channel, the potential sensor is in the S4 and is made up of three arginines (R205, R258 and R261 in hHv1; R201, R204 and R207 in mHv1; R255, R258 and R261 in CiHv1) (Gonzalez et al. 2013) **(Figure 3)**. In this work, for simplicity, we will refer to these arginines as R1, R2 and R3, indicating their relative position.

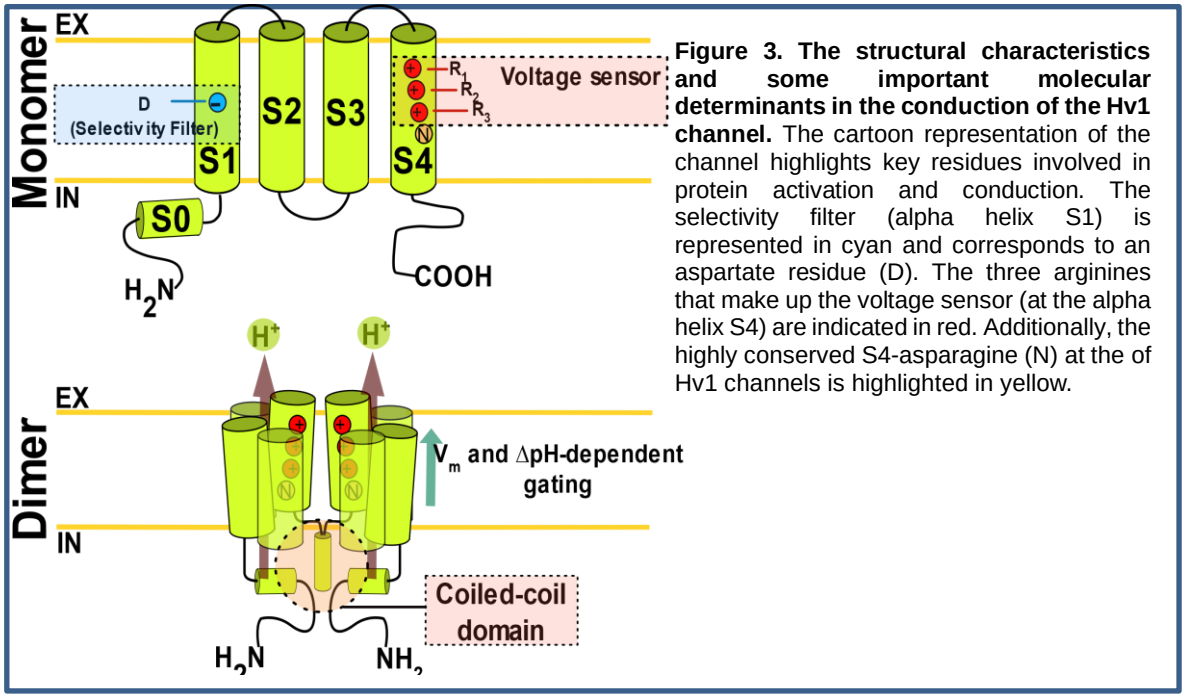


**Figure 3. The structural characteristics and some important molecular determinants in the conduction of the Hv1 channel.** The cartoon representation of the channel highlights key residues involved in protein activation and conduction. The selectivity filter (alpha helix S1) is represented in cyan and corresponds to an aspartate residue (D). The three arginines that make up the voltage sensor (at the alpha helix S4) are indicated in red. Additionally, the highly conserved S4-asparagine (N) at the of Hv1 channels is highlighted in yellow.

The movement of these arginines during channel activation produces a capacitive current that can be recorded with electrophysiological techniques **(Figure 4A)**. These currents are known as gating currents and are a direct measurement of the voltage-sensitive conformational change of the protein during opening (Bezanilla 2018) **(Figure 4A)**. Recordings these gating currents help to answer questions about the phenomena of opening, closing, inactivation, drug sensitivity, pH sensitivity, divalent ion sensitivity, and many other properties of voltage-gated membrane proteins, thus being an interesting experimental approach for understanding the

structure and function of these proteins.

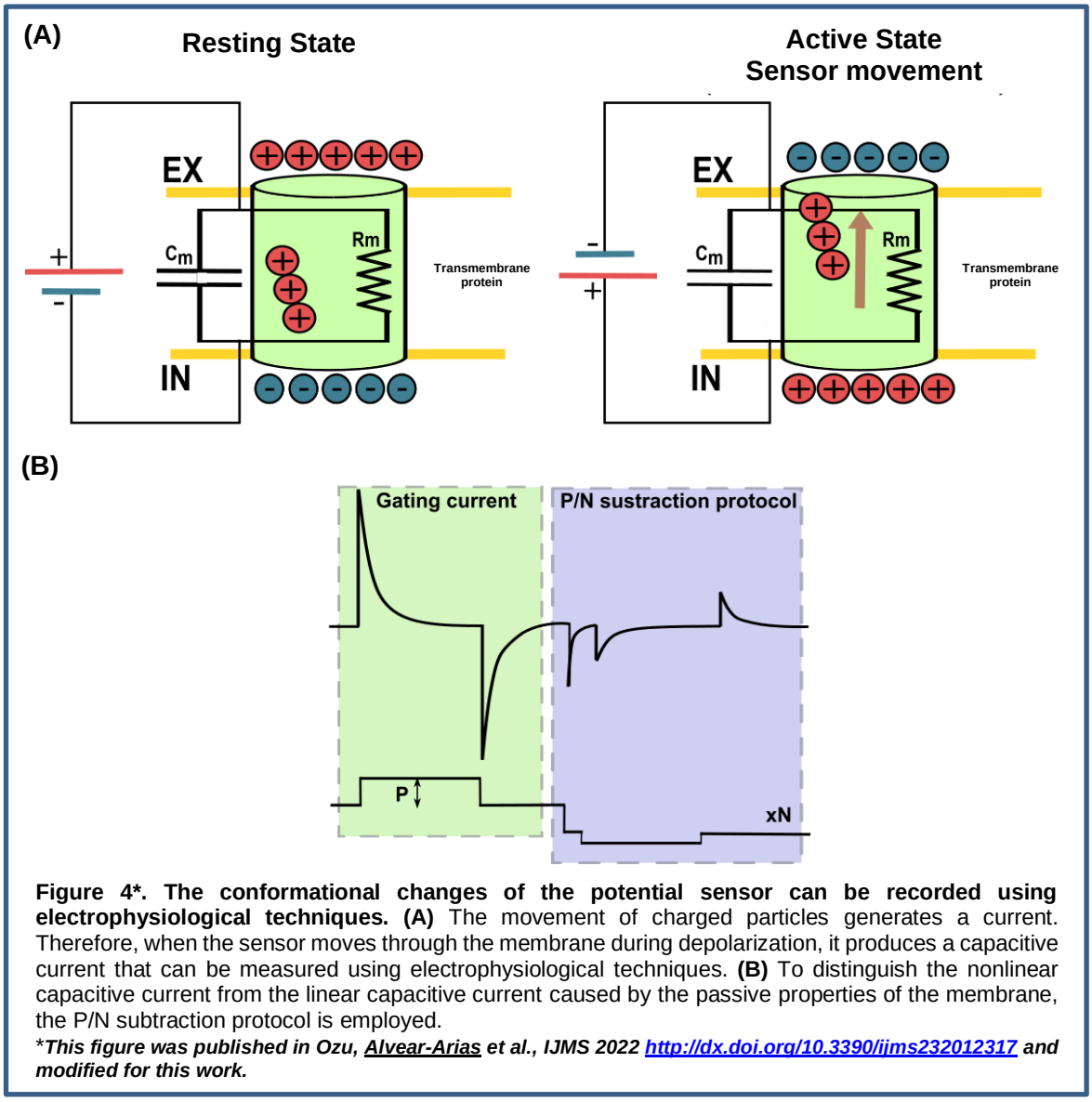


**Figure 4*. The conformational changes of the potential sensor can be recorded using electrophysiological techniques. (A)** The movement of charged particles generates a current. Therefore, when the sensor moves through the membrane during depolarization, it produces a capacitive current that can be measured using electrophysiological techniques. **(B)** To distinguish the nonlinear capacitive current from the linear capacitive current caused by the passive properties of the membrane, the P/N subtraction protocol is employed.

****This figure was published in Ozu, Alvear-Arias et al., IJMS 2022 http://dx.doi.org/10.3390/ijms232012317 and modified for this work.***

The gating currents are nonlinear capacitive currents, which must be subtracted from the linear capacitive currents that emerge from the passive properties of the membrane (Bezanilla 2018; Hille 2001). To do this, a voltage pulse protocol known as the P/N subtraction protocol is used, which consists of applying “N” voltage pulses of opposite polarity to the depolarizing pulse (P) (Bezanilla 2018) **(Figure 4B)**. So that at the end of the pulse protocol application, the linear capacitive current caused by depolarization can be subtracted by subtracting one of equal amplitude generated

by membrane hyperpolarization. Thus, the nonlinear capacitive current corresponds to the movement of the charges of the voltage sensor.

The first detection of the Hv1 channel gating currents was performed in monomeric constructs of *Ciona intestinalis* (ΔNΔC CiHv1) expressed in *Xenopus laevis* oocytes (Carmona et al. 2018). Since the macroscopic proton current is of greater amplitude than the gating current, this ionic component hides the nonlinear capacitive component. To isolate the capacitive current from the macroscopic proton current, the authors of this work used a low-conductive construct, the monomeric mutant ΔNΔC N264R. Thanks to these first measurements, the movement of the protein's voltage sensor during activation was evidenced. From here, the authors reported that the kinetic model of the Hv1 monomer is more complex than a two-state model (*Open*↔*Close*), but rather the sensor at least presents three resting states ($A_1$-$A_2$-$A_3$) with two active states ($B_1$-$B_2$) separated by a large energy barrier between states $A_3$-$B_1$ (Carmona et al. 2018) **(Figure 5).**

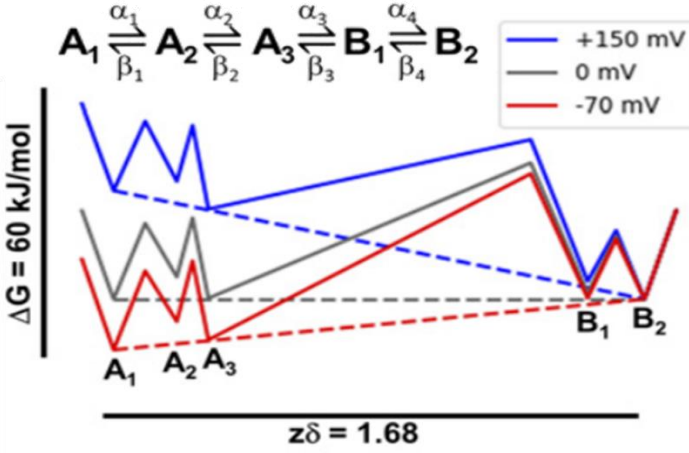


**Figure 5*. A five-state model replicates the sensor movement for the CiHv1 monomer.** A sequential model with five states reproduces the gating currents of the ΔNΔC N264R mutant of CiHv1. Based on measurements, the existence of at least three resting states ($A_1$, $A_2$ and $A_3$) and two active states ($B_1$ and $B_2$) for the monomer sensor could be identified. The figure represents the estimated energy barriers for the five-state model at three different voltages.

The problem with the construct used in that work was that the closing gating current ($B_1 \rightarrow A_3$) presented a slowing of the charge, in which, with short repolarizations, only 1.4% of the total displaced charge during opening was recovered, and 87.6-ms ON-recovery protocols were needed to completely recover the charge (Carmona et al. 2018). Subsequently, a mutant was found that allows the characterization of the gating current (ΔNΔC D160N) without the slowing of the charge (Carmona et al.

2021).

With this new non-conductive construct, clean recordings of the sensor's charge displacement were achieved, allowing for a new experimental approach to answer other questions related to the structure and function of the Hv1 channel, such as pH dependence and proton permeation, which will be discussed below.

## II. The Selectivity Filter and the Channel's Permeation Pathway

The proton channel is a protein that allows the efficient and selective passage of protons through membranes, with a permeability ratio between protons and sodium $P_{H^+}/P_{Na^+} \geq 10^6$ (DeCoursey and Cherny 1994).

Up to date, we know that the selectivity filter (SF) of the proton channel corresponds to the highly conserved aspartate residue of the S1 segment (D112 in hHv1, D160 in CiHv1) **(Figure 6)**. However, until the year 2011 the identity of the SF of Hv1 remained a mystery. Solving this unknown was crucial to answer even deeper questions about the molecular mechanisms related to proton selectivity, the rectifying behavior of the channel, the permeation pathway, and the mechanism of proton conduction.

The first experiments that were crucial in identifying the SF of the Hv1 channel were reported in 2011, almost simultaneously, by two research groups: the work of Berger and Isacoff published in *Neuron* (Berger and Isacoff 2011) and the work of Thomas DeCoursey's group published in *Nature* (Musset et al. 2011).

Berger and Isacoff focused their interest on two positions that initially seemed attractive to them; previous studies predicted that positions R211 (R3) and N214 (a highly conserved asparagine in S4, referred to as N4) were located in the middle of the membrane after the conformational change towards the open state following membrane depolarization (Gonzalez et al. 2010). Berger and Isacoff suggested that these positions could potentially form the pore during the open state.

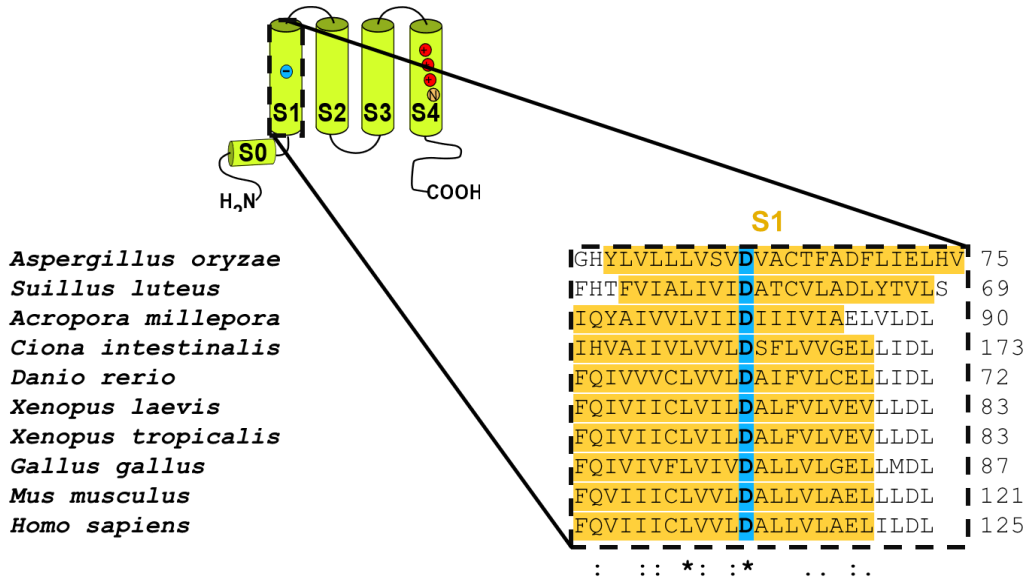


**Figure 6. Alignment of sequences from the S1 alpha helix of Hv1 from various species.** The figure shows the alignment of sequences of the Hv1 channel from different branches of the phylogenetic tree, including fungi (*Aspergillus oryzae* and *Suillus luteus*) and animals such as Ascidians (*Ciona intestinalis*), Amphibians (*Xenopus laevis* and *Xenopus tropicalis*), fishes (*Danio rerio*), birds (*Gallus gallus*) and mammals (*Mus musculus* and *Homo sapiens*). The selectivity filter (D) is highlighted in blue and is highly conserved among species. The amino acids constituting the S4 transmembrane segment are highlighted in yellow.

Therefore, the authors neutralized the charge of R3 (R3S mutant), observing that the channel lost its proton selectivity and acquired permeability to the organic cation guanidinium. By exploring 15 other residue substitutions at the R3 position, all mutations consistently supported the conduction behavior to guanidinium. Thus, the R3 position did not constitute the selectivity filter and, in addition to being part of the voltage sensor, it specifically prevented the permeation of the guanidinium cation. On the other hand, mutating the asparagine N4 to serine (N4S mutant) did not alter the channel's selectivity behavior.

If R3 is positioned in the narrowest part, it should have a countercharge in another transmembrane segment. Based on this reasoning, the authors focused their attention on a highly conserved aspartate (D112 in hHv1), which had previously been predicted by homology modeling to be located in the middle of S1, precisely facing R3 (Ramsey et al. 2010). Thus, using site-directed mutagenesis at D112 position and posterior electrophysiological studies, they determined that the aspartate and

R3 interact by salt bridges, creating a narrow and stable structure in the open state. Charge conservative mutations like D112E maintained the conductive properties, while neutralizing one of the two charges (either D or R) affected the channel's selectivity. Even more interestingly, when the charges were reversed in the double mutant D112R R3D, the construct maintained selective proton conduction. In other words, the interaction through salt bridges between a positive and negative charge in the middle of the protein in its open conformation is determinant for a proton selective conduction (Berger and Isacoff 2011).

Conversely, the group led by Thomas DeCoursey cloned the human gene C15orf27, a protein that contains a voltage-sensing domain that shares 52% similarity with the human Hv1, which includes three arginine residues in the transmembrane segment S4 (Musset et al. 2011). By expressing the product of the gene in HEK-293 cells they observed that the resulting protein was present in the membrane but had no electrical response in patch-clamp experiments. Thus, the molecular elements that differentiate hHv1 and the product of the C15orf27 gene may reside in the residues responsible for proton conduction. Thus, they identified five potential candidates: D112 (D160 in CiHv1), D185, N214 (N4 in the work of Berger and Isacoff; N264 in CiHv1), G215 and S219.

As a result, directed mutations at these five candidates showed that the proton channel conductivity behavior was lost only when the charge of the aspartate at position 112 was neutralized (D112V mutant) (Musset et al. 2011). They performed other D112x-type substitutions showing that the mutations have a small effect on the ΔpH-dependent gating, some affected the kinetics of opening and closing, some more interesting mutations such as D112H, D112A, D112S indicated that the channel lost its selectivity for protons, making it permeable to chloride and methylsulfonate anions ($Cl^-$ and $CH_3SO_3^-$, respectively), while the conservative mutation D112E retained the proton selectivity (consistently with the simultaneously published report from Berger and Isacoff). On the other hand, certain mutations directed to aspartate 185 (another candidate), such as D185M, D185V, D185A, and D185N, resulted in all mutants maintaining selective proton conduction.

The experiments published in 2011 by both research groups finally revealed the mystery surrounding the identity of the selectivity filter (Berger and Isacoff 2011; Musset et al. 2011). Moreover, these experiments support the idea that the SF-R3 interaction constitutes the narrowest segment of the permeation pathway of the channel (Berger and Isacoff 2011), which we now refer to as the constriction zone **(Figure 7)**. Additionally, it was found that the SF not only mediates proton selectivity but also plays a role in charge selectivity (Musset et al. 2011).

Further studies intended to define the structure of the open hHv1 channel by generating homology models for molecular dynamic simulations (Kulleperuma et al. 2013). They used the crystal structures of the KvAP potassium channel's VSD, the paddle chimera, and the NavAB sodium channel's VSD for these simulations because the structural resolution of the channel was not available at the time. These computational predictions suggested salt bridge interaction between the SF and the R2 that results in a necessary charge compensation for proton selectivity (similar to the predicted D112-R3 salt bridge interaction by Berger and Isacoff). Additionally, these simulations proposed that the protein and particularly the permeation pathway of the channel are shaped like an hourglass with intra- and extracellular conically shaped water-filled vestibules (Kulleperuma et al. 2013). These MD simulations also predicted a close interaction between the R3 and the phenyl group of the highly conserved S2 phenylalanine (F150 in hHv1) in the constriction zone (Kulleperuma et al. 2013).

In the same year, an article was published that presented a set of experiments that characterized the conduction features of a series of mutants by changing the position of the aspartate residue along the S1 helix from position 108 to 118 in the hHv1 channel (Morgan et al. 2013). In this study, the authors concluded that positions V109, D112 (SF), and V116 align the hHv1 permeation pathway, which was previously predicted by molecular dynamics (Kulleperuma et al. 2013). These data complemented the emerging studies that investigate the still mysterious permeation pathway of the Hv1 channel. An interesting discovery was that the double mutant D112V V116D displaced the position of the SF. Here, position V116D formed salt

bridges with the R1 (homologous to the salt bridge of the WT channel between D112 and the R3 of the sensor), resulting in a selective proton channel with the same properties as a native Hv1 (Morgan et al. 2013). Therefore, this mutagenesis exploration confirmed that the formation of this environment around the salt bridge interaction is necessary for the channel's proton selectivity.

The year 2013 appeared to be a highly productive period for Hv1 research. Additionally, to the significant articles mentioned earlier, a noteworthy study introduced a family of inhibitory compounds derived from guanidinium benzimidazole pharmacophore (Hong et al. 2013). The authors of this work further elucidated the mechanism by which these compounds bind to the channel, revealing an intracellular binding site in the open state configuration (Hong, Kim, and Tombola 2014). What made these findings particularly intriguing was not only the fact that to that date the only known inhibitors were divalent ions (like $Zn^{2+}$), but the fact that these inhibitors target the permeation pathway in the open state of the proton channel (Hong et al. 2014). Therefore, apart from shedding light on the binding mechanism of this new family of Hv1 inhibitors, this publication provided an opportunity to validate certain hypotheses proposed in earlier studies about the key residues lining the proton permeation pathway. Thus, the residues that mediates the binding was D112 (SF) in S1, F150 (predicted as part of the constriction zone) in S2, S181 in S3 and R11 (R3) in S4 of the hHv1 (Hong et al. 2014) **(Figure 7)**.

In the early part of the year 2014, the Okamura research group published the first X-ray crystallographic structure of a chimeric voltage-gated Hv1 channel (mHv1cc as the authors called) (Takeshita et al. 2014). From this crystal structure, the authors observed that R2 and R3 of the voltage sensor, slid toward the inner-membrane side relative to the highly conserved phenylalanine on S2 (similar to the predicted R3-F150 interaction by Kulleperuma et al., models) (Kulleperuma et al., 2013), which possibly corresponds to a charge-transfer center (Takeshita et al. 2014), as observed in other voltage-gated ion channels (Tao et al., 2010).

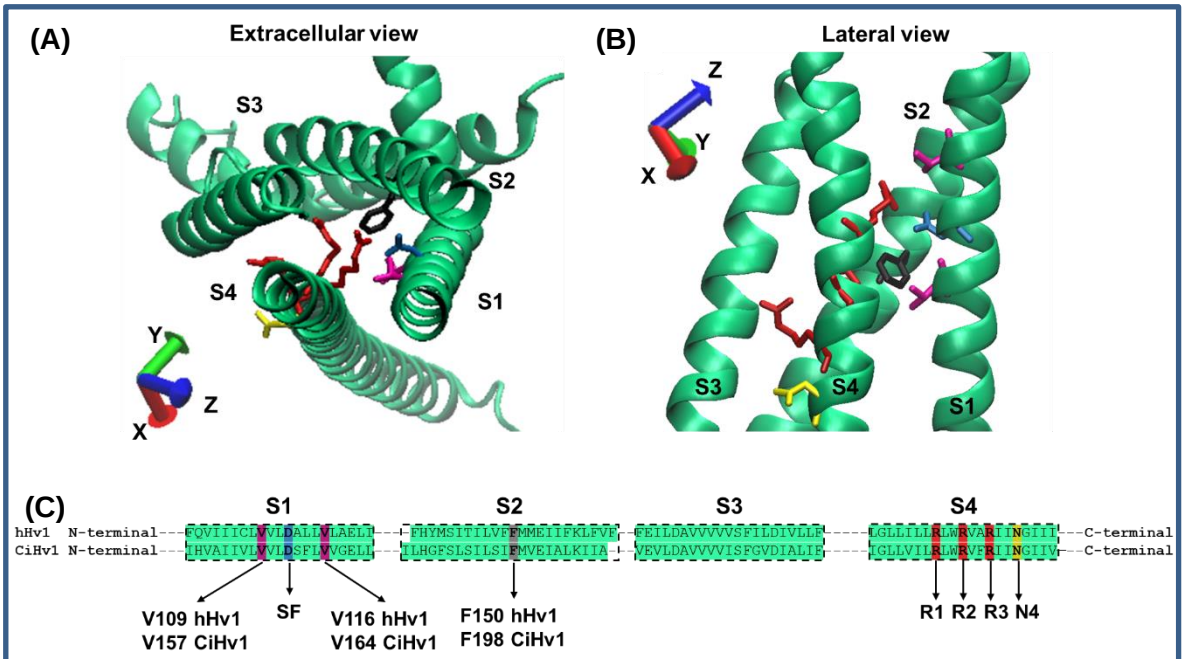


**Figure 7. Residues currently known to be part of the proton permeation pathway of the Hv1 channel. (A and B)** Extracellular and lateral visualization of a close monomeric structural prediction of the human Hv1 channel using AlphaFold V2.0. Both representations highlight the residues constituting the permeation pathway: the selectivity filter (aspartate) is shown in blue, both S1 valines are in purple, the S1 phenylalanine is in grey, the three arginines (R1, R2, R3) constituting the voltage sensor are in red, and the highly conserved S4 asparagine (N4) is in yellow. **(C)** A sequence alignment between hHv1 and CiHv1 transmembrane segments (S1 to S4), highlighting the residues of the permeation pathway with the same color code as in panels A and B.

While key residues involved in the permeation pathway have been identified, the comprehensive composition of the pathway, along with the molecular mechanism of proton permeation, remains unknown. This matter will be extensively discussed in the *Chapter 4* of the *Introduction* section of this doctoral thesis, entitled *"Water and the Controversial Permeation Mechanism of the Hv1 Proton Channel"*.

### III. The pH Sensor

One of the most striking characteristics of the Hv1 channel is its sensitivity to the pH gradient (ΔpH), which is conventionally defined as the difference between the extracellular pH and the intracellular pH ($\Delta pH = pH_{ext}-pH_{in}$) (Cherny, Markin, and DeCoursey 1995). Because of this, the relationship between the macroscopic conductance (G) of the channel as a function of voltage (V), also known as activation curves, shifts towards more negative voltages as ΔpH increases. This inversely

proportional relationship indicates that channels require less energy (voltage) to be activated (Cherny et al. 1995). What is even more intriguing is that the G(V) curves are only affected by ΔpH and not by the absolute pH of the intra- and extracellular solution (Carmona et al. 2021; Schladt and Berger 2020). In practical terms, this means that an activation curve obtained under conditions of $pH_{in}$=5.0/$pH_{ext}$=7.0, will have the same values for the mean activation voltage ($V_{0.5}$) and zδ as one obtained under conditions of $pH_{in}$=4.0/$pH_{ext}$=6.0 because both conditions corresponded to a ΔpH=2 **(Figure 8A)**. However, the kinetics of activation and deactivation are sensitive to the absolute pH **(Figure 8B)** (Carmona et al. 2021; Schladt and Berger 2020).

On the other hand, the unitary conductance of this channel also appears to be sensitive to absolute pH, specifically the intracellular pH, according to measurements obtained by stationary noise analysis (Cherny et al. 2003). The unitary conductance of the human Hv1 channel was estimated to be ~38 pS for both ΔpH=0 ($pH_{in}$=6.5/$pH_{ex}$=6.5) and ΔpH=1 ($pH_{in}$=6.5/$pH_{ex}$=7.5), suggesting that extracellular pH or the gradient established across the membrane has no effect on unitary conductance.

Recent studies measuring gating currents with the mutant ΔNΔC D160N allowed the characterization of the voltage sensor movement under different ΔpH conditions (Carmona et al. 2021). Here, it was reported that the conformational changes of the channel voltage sensor were strongly modulated by ΔpH, with the gating charge displacement (Q) versus voltage (V) relationships shifting towards more negative voltages as the pH gradient increased, like what was observed in G(V) relationships, as well as in the activation kinetics of the gating currents, which are modulated by the absolute pH, but no by ΔpH (Carmona et al. 2021) **(Figure 9).** These observations are tremendously interesting because they suggest that the potential sensor may contain the molecular determinants responsible for the dependence on ΔpH.

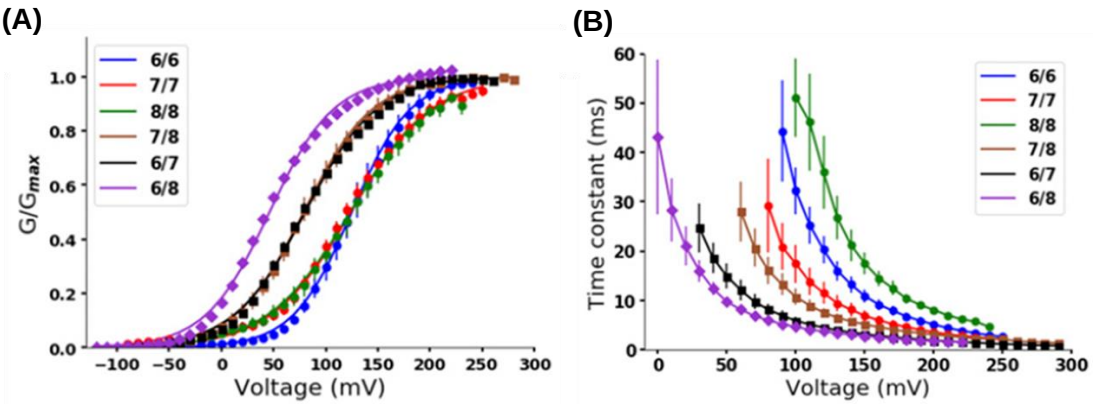


**Figure 8*. Sensitivity to pH of the macroscopic currents of the Hv1 channel. (A)** The G(V) relationship of the macroscopic currents of Hv1 is sensitive to ΔpH. Regardless of the effective concentration of proton in the recording solutions, all curves obtained at a given ΔpH will have the same $V_{0.5}$ y zδ. **(B)** The activation time constants of the channel, on the other hand, are sensitive to absolute pH. For instance, the time constants recorded under conditions of ΔpH=0 (green curve $pH_{in}$=8/$pH_{ex}$=8, red curve $pH_{in}$=7/$pH_{ex}$=7 and blue curve $pH_{in}$=6/$pH_{ex}$=6) have different values.
***This figure was published in Carmona et al., PNAS 2021 https://doi.org/10.1073/pnas.2025556118.***

From the Q(V) and G(V) relationships, they observed that 60% of the energy from the pH gradient is coupled to the voltage sensor movement (Carmona et al. 2021). This calculation was obtained from an empirical expression that describes the total free energy (ΔG) between the coupling of electrical and chemical energy in the form:

$$\Delta G = G_{ex} - G_{in} = \Delta G^0 0 - 2.3\varepsilon RT\Delta pH - zFV$$

This equation represents the charge in the free energy of the system required to move the sensor from its resting state to an active state in the presence of ΔpH across the membrane, as well as in the presence of the membrane's electrical potential. $\Delta G^0 0$ is the difference between the basal energy of the resting and active state. R, T y F are the constants of the ideal gas, the temperature of the system, and the Faraday constant, respectively. The parameter ε describes the chemical potential energy associated with the stabilization of the sensor in its active conformation.

Although there are few studies on the pH sensitivity of the proton channel, the molecular determinants responsible for sensing pH are still unknown.

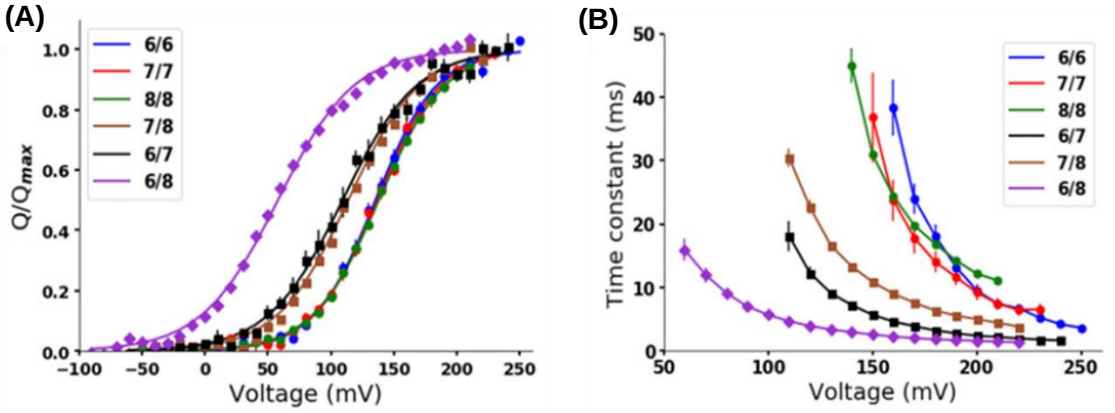


**Figure 9*. pH sensitivity of the gating currents of the ΔNΔC D160N CiHv1 construct. (A)** The Q(V) relationship of the macroscopic currents of Hv1 is sensitive to ΔpH. All curves obtained at a given ΔpH will have the same $V_{0.5}$ value. **(B)** The activation time constants of the channel gating, on the other hand, are sensitive to the absolute pH. For example, the time constants measured under conditions of ΔpH=0 (green curve $pH_{in}$=8/$pH_{ex}$=8, red curve $pH_{in}$=7/$pH_{ex}$=7 and blue curve $pH_{in}$=6/$pH_{ex}$=6) exhibit different values.

**This figure was published in Carmona et al., PNAS 2021 https://doi.org/10.1073/pnas.2025556118.*

## IV. The Proton Depletion Phenomenon

*"Failure is simply the opportunity to begin again, this time more intelligently "*

*-Henry Ford,*

*Founder of Ford Motor Company*

The macroscopic currents of selective proton channels undergo a phenomenon known as proton depletion, which consists of a reduction in the amplitude of the currents over time that becomes more evident at more depolarizing voltages **(Figure 10B)** (De-la-Rosa et al. 2016). Thus, this phenomenon has been observed not only in Hv1 channels recordings, but in other channels like Otopetrin (Otop), and even in omega pores of mutant *Shaker* potassium channels (DeCoursey and Cherny 1996; De-la-Rosa et al. 2016; Starace, Stefani, and Bezanilla 1997; Tu et al. 2018; Zhang et al. 2016). Proton depletion at first may be confused with the slow C-type inactivation process (Hoshi et al., Neuron 1991), pharmacological blockage (Camerino et al., 2007; Hille 2001), or even some types of *run down* seen in certain channels (Becq, Biochim Biophys Acta, 1996). While all of these phenomena may appear similar on an electrophysiological recording, they are caused by wholly different mechanisms.

The slow C-type inactivation process in *Shaker* potassium channels is observed when the fast N-type inactivation process is removed, using the Δ6-46 deletion also known as *Shaker IR* construct (Hoshi et al., Neuron 1991). Recently, a cryo-EM resolution of the W434F *Shaker* IR mutant reveals the mechanism (Tan et al., Sci Adv 2022), unveiling a conformational change that displaces the pore loop (between S5-S6 transmembrane segments) and dilates the ion selectivity filter, preventing channel conduction (Tan et al., Sci Adv 2022; Perozo et al., Neuron 1993; Yang et al., JGP 1997).

On the other hand, *rundown* is a nonspecific event experienced by ion channels, characterized by a time-dependent activity decrease that occurs due to the reduction in the number of channels during electrophysiological measurements. This is mainly caused by the dilution or loss of certain intracellular elements during the experiments (Becq, 1995).

Proton depletion, in contrast, is caused by the nature of proton transport that induces a change in the vicinity of the channels (DeCoursey and Cherny 1996; De-la-Rosa et al. 2016). Due to the extremely low concentration of protons in the physiological (pH 7.2 to 7.4) or experimental context (commonly pH 5.0 to 8.0), a significant reduction in available protons occurs when they are transported through the channels with high efficiency. This results in local changes of intracellular (decreases) and extracellular (increases) concentrations (**Figure 10A)** that conventional buffers employed in electrophysiological recordings can't efficiently replenish (DeCoursey and Cherny 1996). The diffusion coefficient of protons in water is 7000 $\mu m^2 s^{-1}$, whereas for the commonly used buffer HEPES is 500 $\mu m^2/s$ (Agmon, Chem Phys Letters 1995). As a result, a sink effect is produced in the channel's proximity, causing a substantial decrease in the macroscopic proton current **(Figure 10B)**. As can be observed in the representative recording shown in Figure 10, the decrease in current amplitude is a time-dependent phenomenon that becomes more evident at more depolarizing voltages. This is quite interesting because this electrophysiological characteristic is a clear sign of the efficiency with which the Hv1 channel regulates pH conditions in cellular systems, which is key for certain physiological processes where drastic changes in cytoplasmic pH need to be

regulated.

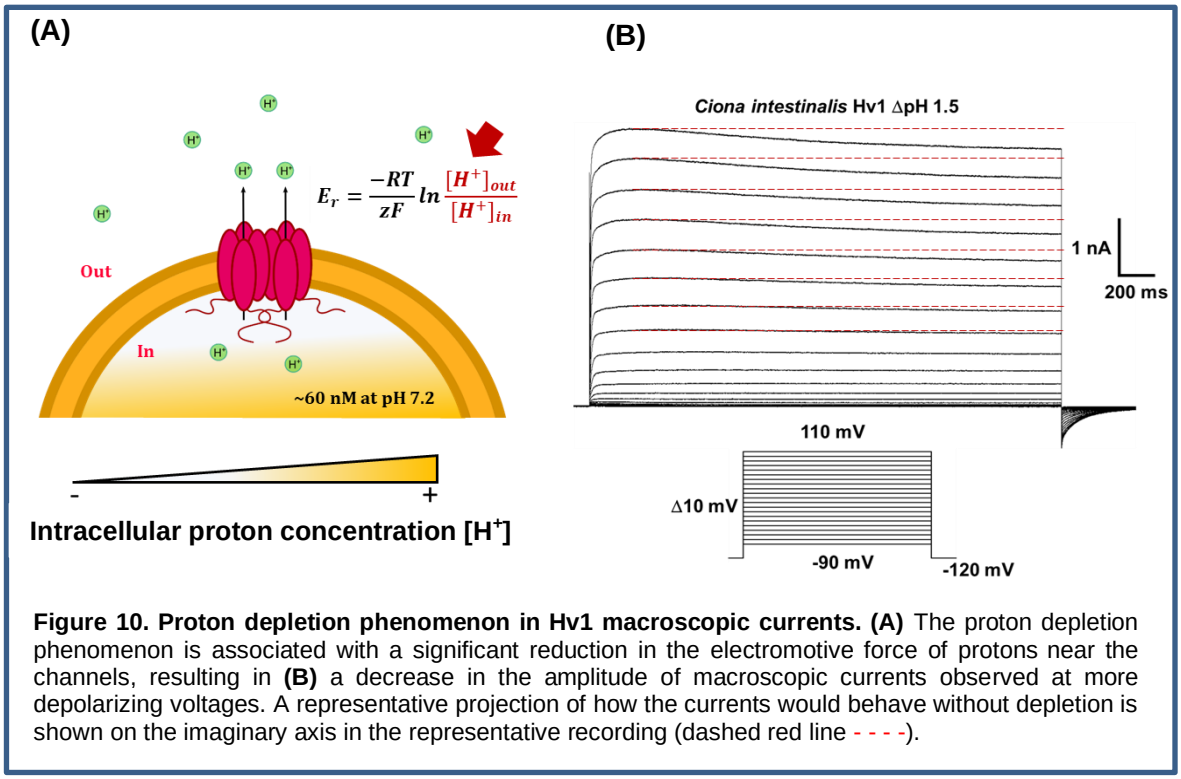


**Figure 10. Proton depletion phenomenon in Hv1 macroscopic currents. (A)** The proton depletion phenomenon is associated with a significant reduction in the electromotive force of protons near the channels, resulting in **(B)** a decrease in the amplitude of macroscopic currents observed at more depolarizing voltages. A representative projection of how the currents would behave without depletion is shown on the imaginary axis in the representative recording (dashed red line - - - -).

The phenomenon of proton depletion poses complications for the recording and analysis of macroscopic proton currents. As mentioned in the previous section, the Hv1 channel is a protein that transports protons selectively. Recall that for any channel that transport an ion selectively, the reversal potential ($E_r$) of the current it conducts it is equal to the equilibrium potential of the transported ionic species, which can be estimated by the *Nernst* potential equation:

$$E_r = \frac{-RT}{zF} ln \frac{[H^+]_{out}}{[H^+]_{in}}$$

However, it is observed in the literature that many published experimental measurements show an evident depletion of protons in their macroscopic currents, and in other cases, the reversal potential estimations of some works vary considerably from the theoretical reversal potential. This currently presents a serious problem for the field of Hv1 channel studies, as depletion complicates the comparison of data obtained between different authors.

# 4) The Controversial Permeation Mechanism of the Hv1 Channel

*"Controversy is a necessary complement to progress "*

*-Friedrich von Schiller,*

*German poet and philosopher*

The voltage-gated proton (Hv1) channel was first cloned in 2006 (Ramsey et al. 2006; Sasaki et al. 2006). In colloquial terms, we could say that the field of research on this protein is quite "young" compared to other transmembrane proteins. Then, there are many unanswered questions, such as the conduction mechanism of protons, which is still a matter of controversy. What is the relationship between water and the conduction mechanism of this protein? To answer this and other questions, some prior information is needed.

## I. Lack of an open structure

The proton permeation in the channel is a topic of debate and still far from being clarified, mainly because the structure of the channel in its open state has not yet been resolved. Currently, there is a 3.45 Å resolution X-ray crystallographic structure of the chimera Hv1 channel (mHv1cc) (Takeshita et al. 2014).

The structure obtained by the Okamura group corresponds to the crystal of the Hv1 channel from mouse (*Mus musculus*), which contains structural elements from two other distinct proteins. These elements were inserted with the intention of increasing the stability of the construct since the native structure of the proton channel is highly flexible. This flexibility has represented a challenge for crystallographers attempting to crystallize it. The inserts were made as follows: the coiled-coil region of the C-terminal was replaced by the leucine-zipper motif from a transcriptional activator GCN4 of brewer's yeast (*Saccharomyces cerevisiae*), inserted to increase the thermostability of the molecule. Additionally, the cytoplasmic region spanning from half of S2 to half of S3 was replaced by its equivalent region from the *C. intestinalis* voltage-sensing phosphatase (CiVSP).

In addition to the chimerizations, the authors removed 74 residues from the N-terminal, and the crystallization was performed in the presence of the $Zn^{2+}$ inhibitor.

Thanks to all these modifications, the authors succeeded in presenting, for the first time (and only), a crystal structure of the Hv1 channel by X-ray crystallography.

The structure showed the formation of trimers, a possible artifact caused by the interaction of the transcriptional activator in the coiled-coil region (Takeshita et al. 2014). Additionally, there are other points against this structure. For example, this chimeric structure forms trimmers, while the native channel forms dimers. This structure also was crystallized in the presence of zinc ion ($Zn^{2+}$), so the authors explained that it was a structure in “Intermediate Resting” (IR) state (Takeshita et al. 2014). All these features are precisely what have led to the lack of consensus when it comes to studying the permeation mechanism. The structure, apart from having low resolution and certain structural inconsistencies with a native Hv1 channel, is coordinating the divalent metal. Therefore, it is a structural state that does not represent either a closed or an open state.

Apart from the mHv1cc structure, there is a nuclear magnetic resonance (NMR) structural resolution of the human Hv1 channel (hHv1) with N- and C-terminal truncations and likewise the Okamura’s structure, it was obtained in the presence of $Zn^{2+}$ (Bayrhuber et al. 2019).

Unfortunately, due to the low resolution of both available structures, it is currently impossible to determine the presence of water molecules from them. For this reason, computational models are built by homology to predict such behavior, and it is here where differences in results and interpretations of the permeation mechanism arise. Prior to the emergence of the X-ray and the NMR structures of the channel, proposed mechanisms were all based on the creation of homology models, whereby protein families with voltage sensors were used as a reference for building these models with available structure resolution. However, since the percentage of identity shared between these proteins is often low, typically around 30% (Pupo et al. 2014), computational predictions derived from these models may not accurately represent the true scenario. Over time, with the emergence of these structures and improvements in computational simulation methods, these models have become increasingly precise and therefore, the predictions and interpretations made from them have been constantly evolving. Currently, two main models are being used to

explain the conduction mechanism of the Hv1 channel which are reviewed below.

### II. Hypothesis one: Grotthuss-like proton conduction throughout the continuum water wire

This model proposes that the channel during the conductive state allows for the formation of a continuum of water molecules (from the intracellular solution to the extracellular solution), where the molecules are arranged forming an “water wire” along the protein (Ramsey et al. 2010) **(Figure 11A)**. Thus, the protons jump between the H-bonds that are formed between the molecules of the water wire (de Grotthuss 2006), something like the *Grotthuss* mechanism, proposed for the conduction of protons in aqueous solution (de Grotthuss 2006), without the need of an explicit titration of residue side chains (Ramsey et al., 2010).

The authors constructed a homology of the Hv1 channel based on the KvAP and Kv1.2-2.1 chimera X-ray crystal structures. In the simulated structure, water molecules in the central Hv1 crevice were observed, revealing a continuous column of water molecules in the center of the Hv1 channel (Ramsey et al., 2010).

Although many homology models have been generated and validated to study the permeation mechanism of the channel, these models have been mainly created using structural templates from other voltage-gated ion channels.

The first characterization of the structural assembly of the Hv1 channel, based on the crystal structure from the Okamura group, was performed by Gianti et al., and from this a model of the active channel was generated (Gianti et al., 2016). In this study, the active models suggested that the hydration profiles of the Hv1 channel are state-dependent, where two highly populated areas of water molecules (corresponding to the two hydrophobic layers of the channel) showed lower water occupancy. However, hydration sites spanned the entire proton permeation pathway (Gianti et al., 2016). Furthermore, in the same work, it was found that the hydrophobic regions of the channel experience density fluctuations, suggesting wet/dry transitions in these hydrophobic environments (Gianti et al., 2016), which have also been observed in other structures (Hummer et al., 2001; Xi et al., 2016; Vaitheeswaran et al., 2004). This suggests that if the permeation pathway of the channel is entirely hydrated, the proton permeation mechanism could be more

complex than a “proton hop” mechanism.

### III. Hypothesis two: the dry constriction zone and the SF protonation

The second model proposes a hypothesis contrary to the previous model. Here it is suggested that the channel during the conductive state forms an interaction of salt bridges between the SF and R2 or R3 of the voltage sensor, which promotes the disruption of the H-bonded water wire (Berger and Isacoff 2011; Dudev et al. 2015; Kulleperuma et al. 2013; Morgan et al. 2013; Sakata et al. 2010) **(Figure 11B)**. This type of interaction would generate the narrowest part of the protein’s permeation pathway, also known as the constriction zone, in which water molecules would not fit due to volume constraints. For this reason, this model establishes that the continuum of water molecules from the intracellular to extracellular bulk solutions would be interrupted by this interaction. In this model, the selectivity filter is protonated to complete the chain of H-bonds, which protons use to move during conduction in this channel.

**Model 1:** Proposes a water wire along channel that allows for *Grotthuss*-like *proton transport.*

**Model 2:** Proposes a protonation of SF with interruption of water wire

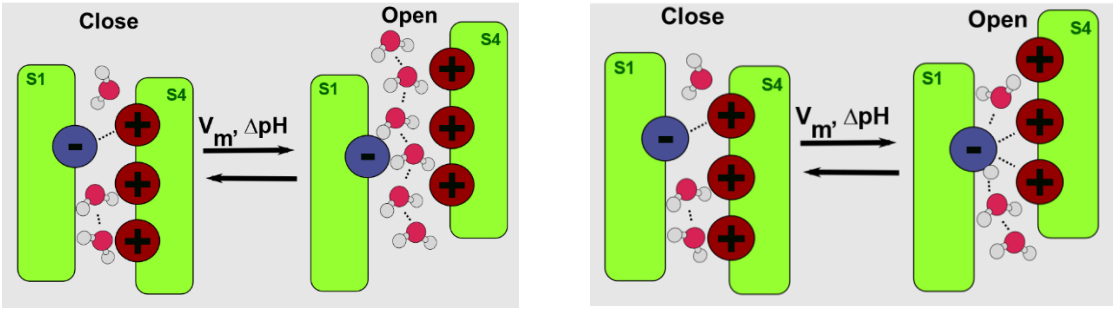


**Figure 11. Proposed models for proton conduction in the Hv1 channel.** Currently, two models exist to explain proton conduction in the Hv1 channel, with opposing mechanisms. Model 1 suggests that when the channel is open, a continuum of water molecules is established through which protons jump in a manner similar to the Grotthuss mechanism, by hopping between the H-bonds formed among the molecules of the water wire. On the other hand, model 2 posits that the continuum of water molecules is disrupted by the interaction of salt bridges between the selectivity filter and the second or third arginine residues that constitute the voltage sensor. In this model, the aspartate residue is protonated to complete the chain of H-bonds that protons utilize as a permeation pathway.

### IV. Interesting evidence that deserves attention

The problem with the models is that they do not satisfy entirely the experimental observations. Okamura’s crystallographic structure uncovered the presence of two

hydrophobic shield layers in the Hv1 channel (Takeshita et al., 2014). One of these layers is located near the inner/cytoplasmic vestibule and contains the highly conserved S2 phenylalanine predicted as the charge-transfer center, while the second layer is positioned slightly above R1, towards the extracellular vestibule. Between these two layers, near to the constriction zone of the channel, a confined space was observed which contains water molecules sandwiched between the hydrophobic shield layers (Takeshita et al., 2014). Moreover, the structure reveals an interesting issue: R3 is oriented toward the external region of the protein and is situated such that it can interact with N4. It has been widely reported that mutations that involve charge addition to this highly conserved asparagine **(Figure 12)** dramatically affect Hv1's conducting properties. For example, when N is mutated to R **(Figure 13)**, proton conduction decreases significantly (Carmona et al. 2018; Qiu et al. 2013; Randolph et al. 2016; Sakata et al. 2010). This residue, being highly conserved, and the evidence indicating that mutations to this residue alter channel conductance, suggests that this asparagine may play a role in the proton permeation mechanism.

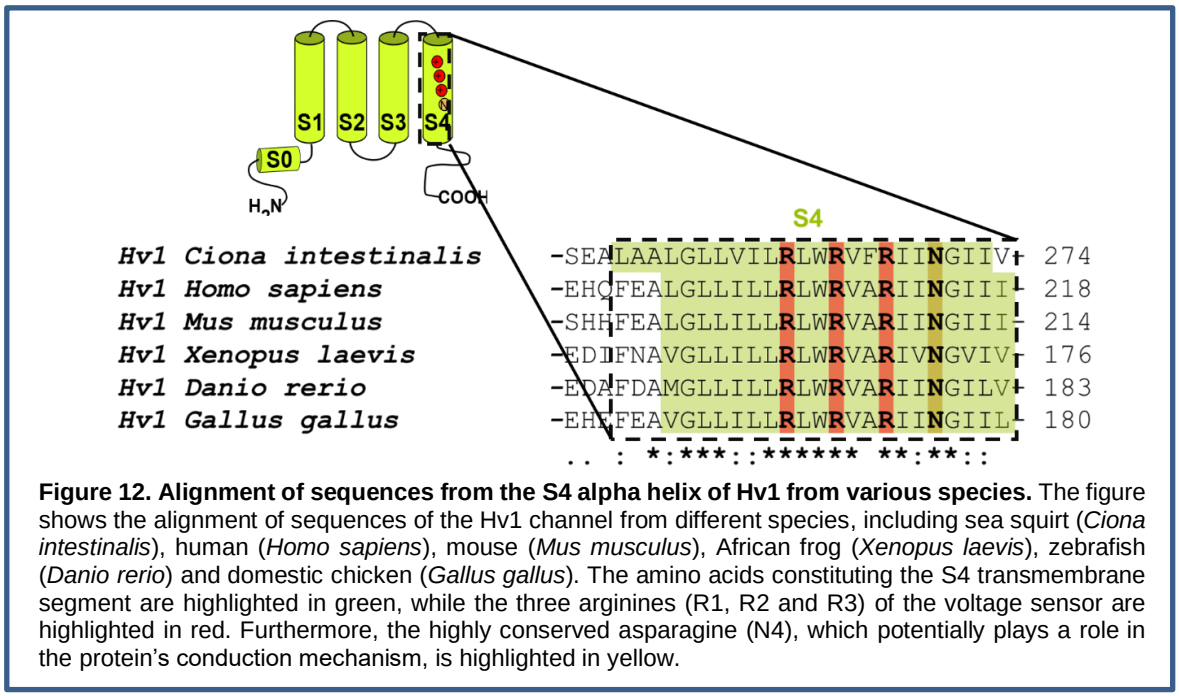


**Figure 12. Alignment of sequences from the S4 alpha helix of Hv1 from various species.** The figure shows the alignment of sequences of the Hv1 channel from different species, including sea squirt (*Ciona intestinalis*), human (*Homo sapiens*), mouse (*Mus musculus*), African frog (*Xenopus laevis*), zebrafish (*Danio rerio*) and domestic chicken (*Gallus gallus*). The amino acids constituting the S4 transmembrane segment are highlighted in green, while the three arginines (R1, R2 and R3) of the voltage sensor are highlighted in red. Furthermore, the highly conserved asparagine (N4), which potentially plays a role in the protein's conduction mechanism, is highlighted in yellow.

## 5) The Close Relationship Between Asparagine and Water Configuration

*"All great discoveries, indeed, all great ideas, have involved comparison "*

*-Isaiah Berlin,*

*British philosopher*

To understand the relationship between the conduction mechanism of the Hv1 channel and the possible role played by the highly conserved asparagine of the S4 alpha helix, a good exercise would be to evaluate the role played by asparagine residues in proteins specialized in water transport, such as aquaporins **(Figure 14)**. Aquaporins are a large family of transmembrane proteins that allow efficient transport of water and small solutes and are expressed in virtually all living organisms (Ozu et al. 2018). Each monomer of this protein is composed of six transmembrane segments (TM1 to TM6), with N- and C-terminals in the cytoplasmic domain. In the intracellular loop B and the extracellular loop E, the NPA motifs are found (named because they are composed of an asparagine, a proline and an alanine) **(Figure 14A)** (Ozu et al. 2018), which are highly conserved in the aquaporin family and are crucial for water conduction in these proteins (as we will see below), precisely due to the presence of both asparagine residues.

The water conduction mechanism in AQPs is well studied thanks to the availability of high-resolution structures (unlike the Hv1 channel), which have allowed visualization of water molecules in the protein (Ozu et al. 2022). Thus, using these structures together with computational simulation techniques, it is known in detail how water molecules interact with the protein as they are transported.

Water molecules travel in single file along the permeation pathway, and this conduction is tremendously efficient. This is due to one of the walls of the pore being composed of hydrophobic amino acids side chains, which reduces friction between the pore and the transported molecules, while on the other side of the pore, the water molecules encounter residues that offer H-bonding via carboxyl groups **(Figure 14C)**. When the water molecules being conducted reach the central region of the protein, they encounter asparagines from the NPA motifs of loops B and E. These asparagines form H-bonds with the water molecules, causing a rotation of their

dipole **(Figure 14C).** This rotation is crucial as it plays a role in excluding protons. By rotating the dipole angle, the formation of H-bonds between neighboring water molecules being conducted is disrupted. This interruption prevents the potential conduction of protons through the aligned water molecules within the aquaporin channel (Ho et al. 2009; Ozu et al. 2018).

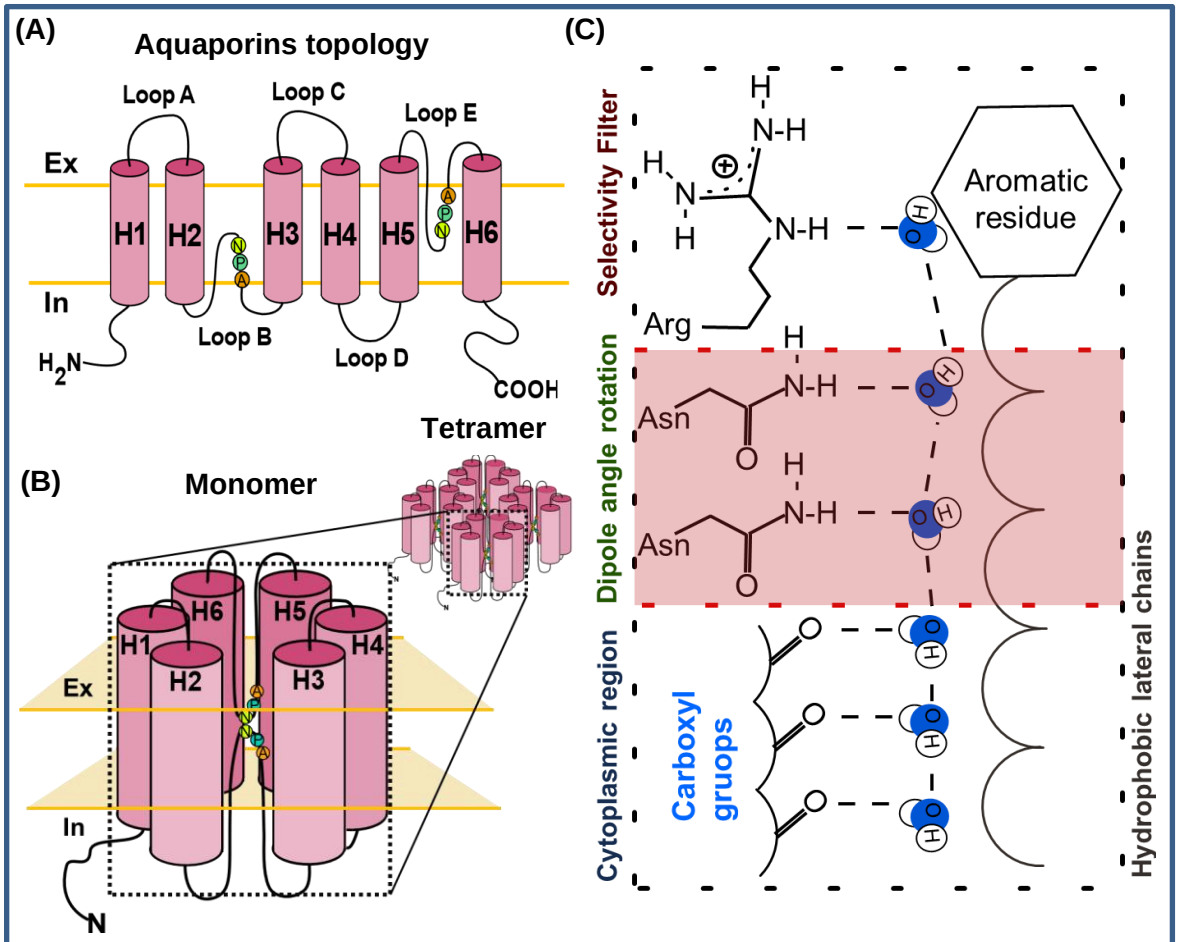


**Figure 14. Topology and mechanism of water conduction in aquaporins. (A)** Each monomer of an AQP consists of six transmembrane segments (H1-H6), with C- and N-terminals located in the cytoplasmic domain. Loops B and E contain the NPA motif and these are embedded in the lipid membrane. **(B)** The NPA motifs of each loop are positioned at the center of the membrane. **(C)** Water molecules are conducted in a single file within the AQPs. When the water molecules reach the protein's equator, they encounter both asparagines of the NPA motif. At this point, they form hydrogen bonds and undergo a rotation of the NPA motif, facilitating the coordination through H-bonds. This rotation plays a crucial role in proton exclusion, making it difficult the formation of H-bonds between water molecules that proton use to conduct themselves.

Aquaporins serve as a prime example highlighting the significance of asparagines as molecular components that must be taken into consideration when evaluating the arrangement of water molecules in the permeation pathways of transmembrane proteins.

# Hypothesis

“Water molecules in the constriction zone of the Hv1 channel acquire a specific configuration (i.e., hydration profile and dipole orientation angle) that modulates proton conduction. This water configuration is modulated by residue N264 in CiHv1”.

# Aim

To understand how the nature of water molecules -i.e., hydration profile, dipole angle configuration and water permeability- is modulating the proton conduction in CiHv1 channel by studying the N264 residue.

# Goals

1. To investigate the impact of some charge mutations at the N264 site on the conductive properties of the CiHv1 channel using patch-clamp techniques, applying a quantitative method to discriminate proton depletion.

2. To analyze the movement of water, hydration profiles, and dipole angle configurations in both the CiHv1 channel and mutant versions at the N264 site using molecular dynamics simulations.

3. To analyze volume changes in wild type and mutants Hv1-expressing oocytes under hypoosmotic conditions and evaluate the water fluxes.

# Materials and Methods

## 1) Mutagenesis, Transcription, and Sequencing

The N264R and N264E mutations were introduced using the QuikChange kit (Promega Corp) into a Hv1 sequence from *Ciona intestinalis* (CiHv1) contained in a pSP64T vector kindly provided by Dr. Yasushi Okamura of Osaka University, Osaka, Japan. The mutant DNA was amplified by PCR, verified by sequencing, and then linearized with pvuII restriction enzymes. In vitro transcription was performed using the mMESSAGE mMACHINE kit (Ambion) with the SP6 RNA polymerase enzyme, following the manufacturer's instructions. RNA was quantified by absorbance at 260 nm and verified for integrity by agarose gel electrophoresis at 1%.

## 2) Extraction of *Xenopus laevis* Oocytes and RNA Injection

The *X. laevis* oocytes were surgically obtained by an abdominal incision of the adult animal and then treated with type IV collagenase, following the methodology previously described in the literature (Alvarez et al. 2019). The oocytes are then injected with 50 nL of RNA at a concentration of 1 mg/mL in oocyte ringer 2 (OR2) calcium-free and then incubated in ND96 medium at 18°C for 24 to 48 hours for electrophysiological recordings, using a methodology that was previously standardized (Carmona et al. 2018, 2021). The composition of the OR2 buffer was: 82.5 mM NaCl, 2 mM KCl, 1 mM MgCl2, 5 mM HEPES supplemented with 0.3 mg/mL amikacin, 10 U/mL penicillin, and 10 mg/mL streptomycin. The pH of the solution was adjusted to 7.4 and then sterilized by filtration. The composition of the ND96 buffer was: 96 mM NaCl, 2 mM KCl, 1.8 mM CaCl2, 1 mM MgCl2, 5 mM HEPES supplemented with 0.3 mg/mL amikacin, 10 U/mL penicillin, and 10 mg/mL streptomycin. For oocyte maintenance after RNA injection, it was also supplemented with 2.5 mM sodium pyruvate. The pH of the solution was adjusted to 7.4 and then sterilized by filtration.

## 3) Electrophysiological Recordings

### I. Inside-out Patch-clamp Technique

The *inside-out patch-clamp* technique (Neher and Sakmann 1992) was used to record the macroscopic currents produced by the proton channel expressed in membrane patches of *X. laevis* (Alvarez et al. 2019; Carmona et al. 2018, 2021). The Ag/AgCl reference electrode was connected to the bath solution through a 1% agar bridge made in a 3 M KCl solution and this was grounded. The electrical contact with the pipette solution was made through an Ag/AgCl electrode. Before forming the seals, the potential difference between the two electrodes was compensated using the AxoPatch 200B operational amplifier (Axon Instruments) using the pipette offset command. Once the electrical seal between the recording pipette and the oocyte membrane was formed (also known as cell-attached configuration), the capacitances were compensated. Subsequently, the patch was excised to obtain the inside-out configuration. All assays were performed at room temperature (20°C) controlled with an air conditioning system. The recording micropipettes were fabricated with a programmable puller, model P-97 (Sutter Instruments, Co.) using borosilicate capillaries (World Precision Instruments, Inc.) and polished with a microforge (Microforge MF-830, Narishige, Co.) obtaining pipettes of ~15 μm with resistances in the range of 1 to 1.5 MΩ.

### II. Recording Acquisition

The recording chamber made with a transparent acrylic plate was mounted on an anti-vibration table, under a binocular microscope. The movement of the pipette was controlled with a mechanical micromanipulator. The AxoPatch 200B amplifier (Axon Instruments) was used for a voltage-clamping the membrane and the analog signals were digitized at 16-bit with a Digidata 1440A (Axon Instruments) and acquired using the voltage pulse generation program Clampex 10.7. The signal was offline filtered at 10 kHz with a Bessel-type digital filter with 8 low-pass poles using the analysis software Clampfit 10.7.

### III. Recording Solutions

The solutions used were optimized for recording proton currents, avoiding the presence of ionic species such as $Na^+$, $K^+$ or $Ca^{2+}$, that could induce macroscopic currents of channels that are expressed endogenously in the expression system. The composition of the solutions adjusted to pH 5.0 and pH 6.0 was as follows: 100 mM of the acid buffer 2-(N-morpholino)ethanesulfonic acid (MES), 2 mM $MgCl_2$, 1 mM ethylene glycol-bis(b-aminoethyl eter)-N,N,N',N''-tetraacetic acid (EGTA), and 50 mM N-methyl-D-glucamine (NMDG) – methane sulfonic acid ($MeSO_3$). For the solutions adjusted to pH 7.0, the composition was: 100 mM of the acid buffer 4-(2-hydroxyethyl)-1-piperazineethanesulfonic acid (HEPES), 2 mM $MgCl_2$, 1 mM EGTA and 50 mM NMDG-$MeSO_3$. The osmolarity of the solutions with this composition were about 190-200 mOsm.

### IV. Obtention and Analysis of Macroscopic Currents: G/Gmax vs Voltage (GV) Relationships

A variable duration pulse protocol was used, ranging from -90 mV to +130 mV in 20 mV increments, with a suitable duration for each record to reach the steady state. The $G/G_{max}$ values were plotted as a function of voltage. This relationship was fitted to a Boltzmann function for a two-state model of the form:

$$\frac{G}{G_{max}} = \frac{1}{1+e^{\frac{z\delta F(V_m - V_{0.5})}{RT}}} \qquad (Equation\ 1)$$

Where zδ is the apparent charge fraction that moves in the electric field, F is Faraday's constant, $V_m$ is the membrane potential, $V_{0.5}$ is the voltage at which the channel has a probability of opening equal to 0.5, R is the gas constant, and T is the temperature. $G_{max}$, zδ and $V_{0.5}$ are free parameters used to fit the function.

### V. Obtention and Analysis of Macroscopic Currents: Ionic Selectivity of the Hv1 Channel Using a Fast Ramp Pulse Protocol

Recordings were obtained for the reversal potential analysis using a fast-ramp pulse protocol, standardized to avoid proton depletion (De-la-Rosa et. al., 2016).

The results obtained were compared with the values predicted by the Nernst

equation for a proton-selective channel:

$$E_r = \frac{-RT}{zF} ln \frac{[H^+]_{out}}{[H^+]_{in}} \qquad (Equation\ 2)$$

Where R is the gas constant, T is the temperature, z corresponds to the elementary charges of the ion, F is the Faraday constant, $[H^+]_{out}$ is the extracellular proton concentration, and $[H^+]_{in}$ is the intracellular proton concentration. The proton concentration was calculated from the recording solutions calibrated pH:

$$pH = -log_{10}[H^+] \qquad (Equation\ 3)$$

## VI. Obtention and Analysis of Macroscopic Currents: Non-stationary Noise Analysis for Unitary Conductance Estimations

For non-stationary noise analyses (Sigworth 1980), a depolarizing pulse was applied with a duration of 2000 milliseconds, which was repeated at least 200 times. From the resulting current traces, 8000 isochrones are obtained, from which the mean current ($\underline{I}$) and variance ($\sigma^2$). The recordings were filtered at ½ of the sampling frequency. The variance as a function of the mean current was fitted to a parabola of the form:

$$\sigma^2 = i\bar{I} - \frac{\bar{I}^2}{N} \qquad (Equation\ 4)$$

Where i corresponds to the unitary current and N to the number of channels. To correct for equipment noise (current fluctuations that occur while the channels are closed), the $\sigma^2$ produced by these fluctuations was subtracted from the $\sigma^2$ of the current traces produced by the opening of the channels.

To ensure that channel rundown or proton depletion did not affect the calculation of the variance, the difference between successive pulses ($y_i$) along the isochrone was used to correct deviation of the variance:

$$y_i = \frac{1}{2}(x_i - x_{i+1}) \qquad (Equation\ 5)$$

The points along the isochrone are represented by $x_i$ and $x_{i+1}$ represents the successive point to $x_i$.

After this conversion, the variance is given by the expression:

$$\sigma_I^2 = \frac{2}{N-1}\sum_{1}^{N}(y_i - \bar{y})^2 \qquad (Equation\ 6)$$

Where N is the number of times the voltage protocol was applied. The unitary conductance value (g) can be calculated using the unitary current value (i) obtained from the linear fit to the initial slope of the parabola:

$$y = \frac{i}{(V_m - E_r)} \qquad (Equation\ 7)$$

Where $V_m$ is the membrane voltage and $E_r$ is the reversal potential.

# 4) Molecular Dynamics Simulations

## I. Generation of Comparative Models

To assess the hydration profile, dipole angles of the water molecules and surface electrostatic profile, we created comparative models of the monomeric ΔNΔC voltage-gated proton Hv1 channel of *C. intestinalis*. The monomeric construct encompasses the residues 136 to 269 of the total length of CiHv1 channel (Carmona et al. 2021). These models were based on the X-ray crystal chimera structure obtained by Okamura´s group PDB 3WKV (Takeshita et al., 2014). The models were built using MODELLER v. 9.22 software (Webb and Sali 2016). The obtained homology model of the WT channel was in the Intermediate Resting (IR) described by the authors of the crystal; thus, an Active (A) state model was generated by shifting the sequence alignment three positions towards the N-terminus, emulating a ~0.5 nm displacement of the S4 helix towards the extracellular side; a methodology that has been previously used by our laboratory and others (Carmona et al. 2021; Gianti et al. 2016). The sequence similarity between the structure template and the CiHv1 construct sequence is 40%.

Missing regions from the template (such as the VIIVPHGNPA and the VGESEA motifs) were added using the loop modeling module of MODELLER v 9.22 (Carmona et al. 2021; Webb and Sali 2016). Finally, the models with the lowest Discrete Optimized Protein Energy (DOPE) score were selected (Shen and Sali 2006). Subsequently, the N264E and N264R mutants were generated for both IR and A

states by using the VMDv1.9.3 software (Humphrey and Schulten, 1996).

## II. Molecular Dynamics Simulations of the Active Generated models

Molecular dynamics (MD) simulations were performed with the NAMDv2.12 software (Phillips et al., 2005) and the CHARMM32 force field (Best et al. 2012; Mackerell et al. 1998), employing periodic boundary conditions in explicit solvent TIP3P water model (Jorgensen et al., 1983) and a POPC membrane with a box of size 100x100x70 $Å^3$ (X, Y, Z axis, respectively). The membrane plane was aligned along the X-Y axes of the periodic box. A 12 Å cut-off sphere was used for real-space-long-range interactions, with a smoothing function applied between 10 to 12 Å. Temperature was controlled at 310 K using a Langevin thermostat with a friction factor of 1 $ps^{-1}$. Pressure was regulated by a Langevin piston coupled to the Nose-Hoover algorithm at 1 atm (Martyna, Tobias, and Klein 1994). For the calculation of electrostatic interactions along the periodic box, the Particle-Mesh-Ewald method was used (Darden, York, and Pedersen 1993). All bonds involving hydrogens were constrained to their equilibrium distance using the SHAKE algorithm (Ryckaert, Ciccotti, and Berendsen 1977). Prior to the simulations, a minimization and thermalization was run. Subsequently, 150 ns of simulation data were collected for each model and their respective mutants (CiHv1 WT, N264E y N2564R in the IR and A states), and the first 50 ns of simulation were discarded.

All CiHv1 structures from the trajectories were structurally aligned with reference to a template structure. This alignment was performed to ensure that the cannel's permeation pathway was aligned along the Z-axis, with its center (D160 residue, the selectivity filter) located at the origin (Z= 0 Å). The structural stability of each dynamic was evaluated using the Root Mean Square Deviation (RMSD):

$$RMSD = \sqrt{\frac{\sum_{i=1}^{N}(x_i - \hat{x}_i)^2}{N}} \qquad (Equation\ 8)$$

Where $\hat{x}_i$ represents the position of each alpha carbon of the protein, and $x_i$ is a reference position, which in this case is the initial configuration. $N$ is the total number of alpha carbons in the system.

### III. Calculation of the Hydration Profiles and Orientation of the Dipole Angle of Water Molecules Along the Permeation Pathway of CiHv1

For the calculations of water densities or channel hydration profiles, the average number of water molecules found in each bin during the 100 ns simulation was computed: the relative probability ($p$) of finding a water molecule in each bin of the protein's Z-axis is given by:

$$p = \frac{P}{P_0} \qquad (Equation\ 9)$$

$P$ is the average number of water molecules found in each bin, and $P_0$ is the number of water molecules found in the same volume in solution (bulk).

The water dipole moment orientation is given by:

$$\vec{\mu}(\vec{r}, q) = \sum_{i=1}^{n} q_i(\vec{r}_i) \qquad (Equation\ 10)$$

$$\theta_z = arccosine \frac{\vec{\mu}_z}{|\vec{\mu}_i|} \qquad (Equation\ 11)$$

Where $q_i$ and $\vec{r}_i$ are the partial charges and positions of each atom of the water molecule; $\vec{\mu}_i$ is the dipole vector of the water molecule pointing along the direction of the Z-axis of the channel, $|\vec{\mu}_i|$ is the magnitude of the dipole vector of the water molecule.

For both water molecule density calculations and dipole angle orientation, a cylinder of 20 Å in length and 3 Å in diameter along the Z-axis was used. The cylinder position was taken from min= -26 with a usage of 50 bins.

### IV. Calculation of the SF-R2 and SF-R3 distances

The interaction between the selectivity filter and R2 and R3 through salt bridges was assessed by measuring the distance between these amino acid pairs. A distance of ≥ 4 Å was considered indicative of a salt bridge, based on previous

literature computations (Sinha et al. 2007). In the CiHv1 WT, N264E and N264R models, the distances between D160-R255 (SF-R2) and D160-R258 (SF-R3) were calculated. The distance (d) between amino acids was determined by calculating the modulus of the resultant vector obtained from the difference in positions of the alpha carbon of each amino acid's side chain in three-dimensional space, represented by the vectors $P_1 = (X_1, Y_1, Z_1)$; $P_2 = (X_2, Y_2, Z_2)$ corresponding to each amino acid:

$$d(P_1, P_2) = \sqrt[2]{(X_2 - X_1)^2 + (Y_2 - Y_1)^2 + (Z_2 - Z_1)^2} \quad (Equation\ 12)$$

## 5) Determination of the osmotic permeability coefficient in *Xenopus laevis* oocytes

The osmotic permeability of oocytes injected with CiHv1 and the N264E and N264R mutants was determined from volume changes registered by videomicroscopy.

The experiments were performed 48 hs after the injection, by applying two gradients simultaneously in the same solution. One of them was to set the driving force for transmembrane water movement. The other one was to increase the open probability of CiHv1 and mutants, in order to set the channels into a conducting state. The isosmotic solution was ND96 at pH 9.4 (200 mosmol.$Kg_w^{-1}$). Then, the hypoosmotic solution was developed by a 1/5 dilution of ND96 (40 mosmol.$Kg_w^{-1}$) and the pH set to 9.4. The osmotic gradient was established by changing the isosmotic solution by the hypoosmotic one. In this way, each experiment was performed under a 160 mosmol.$Kg_w^{-1}$ osmotic gradient, simultaneously with a pH gradient of 2 ($\Delta$pH2; assuming an oocyte intracellular pH of 7.4), a condition that increases the open probability of CiHv1 proton channels (Carmona et al., 2021). The volume time course was recorded by means of videomicroscopy, by using the high-resolution camera of the cell phone mounted on a binocular microscopy. The experiments were recorded at 30 fps in 1-minute long mp4-format videos. The analysis of the experiments was performed by assuming the spherical shape of the oocyte cell. The ImageJ software was used for automatic analysis of the images to obtain the circular area of the oocyte in each frame. Next, Microsoft Excel was used

to work with the numerical data obtained from the images.

According to the osmotic law (Equation 13), the water flux ($J_W$) is proportional to the osmotic permeability coefficient ($P_f$), the membrane surface area ($A$), the molar volume of water ($V_W$), and the osmotic gradient ($\Delta osm$):

$$P_f = \frac{J_W}{V_W \cdot A \cdot \Delta osm} \qquad (Equation\ 13)$$

By assuming that oocytes have a spherical shape, and that $J_w = \frac{dV}{dt}$, then $J_W$ can be determined by linear fitting of the volume time course at the beginning of the osmotic response. Then, Pf can be determined from the experimental data (Ozu et al. 2013).

Data were presented as mean ± SEM. Normality were proven for all data sets. ANOVA and unpaired Student's t-test were applied. A *P* value of $P < 0.05$ was considered statistically significant.

# Results and Discussions

## 1) Standardization of the Protocol for Controlling pH During Electrophysiological Recordings in CiHv1

It is evident that pH control is key to obtaining records of macroscopic currents with this channel. To achieve this, some experimental considerations can be taken to avoid or reduce proton depletion and thus increase the reliability of macroscopic current records of the Hv1 channel. One of these considerations is the fast ramp voltage protocol, which allows an estimation of the reversal potential (thus providing knowledge of the experimental pH conditions) (Alvear-Arias et al. 2022; Carmona et al. 2021; Zhao and Tombola 2021).

Standardization of the protocol for controlling pH during electrophysiological recordings in CiHv1 is crucial for studying the conductive properties of the proton channels. As mentioned in the *Introduction* (See *Chapter 3, Section IV: The Proton Depletion Phenomenon*), macroscopic proton currents suffer proton depletion, which alters the local pH concentrations and affects experimental conditions. The biophysical properties of proton channel currents are highly modulated by the pH gradient established across the membrane. Therefore, it is important to establish an experimental methodology that ensures the reproducibility of electrophysiological experiments before starting an experimental run with the Hv1 channel. To address this, a fast-ramp voltage pulse protocol was standardized to estimate the experimental $E_r$ before and after each voltage pulse protocol, mainly to obtain GVs curves. This allows us to determine whether there were any local pH variations during each of the experiments conducted. This methodology proposes a solution to the systematic problem presented in published proton current studies. Proper calibration of the fast-ramp protocol is necessary for this purpose. Therefore, before proceeding with the functional characterization of Hv1 and the mutants proposed for studying conductive profiles at the N264 position, the work performed on standardizing the method will be presented.

The fast-ramp pulse protocol is designed to minimize proton depletion during macroscopic current acquisition and consist of two important steps: (1) Pre-pulses of depolarizing voltage, and (2) the fast voltage ramp **(Figure 15)**. In the first part of the protocol, a family of depolarizing pulses is applied at different voltages. The important detail is that these pulses do not need to reach steady-state currents, but rather its application is intended to set the channels contained in the membrane at different open probabilities ($P_O$) before the application of the fast voltage ramp. This step is crucial because the application of short depolarizing pulses prevents excessive proton efflux, and thus experimental pH conditions are minimally altered. Subsequently, after the application of the pre-pulses, all traces are brought to the same potential from which the membrane voltage descends in a fast ramp **(Figure 15)**. The fast ramp also implies a very short proton flux during the experiment, which contributes to the maintenance of pH conditions.

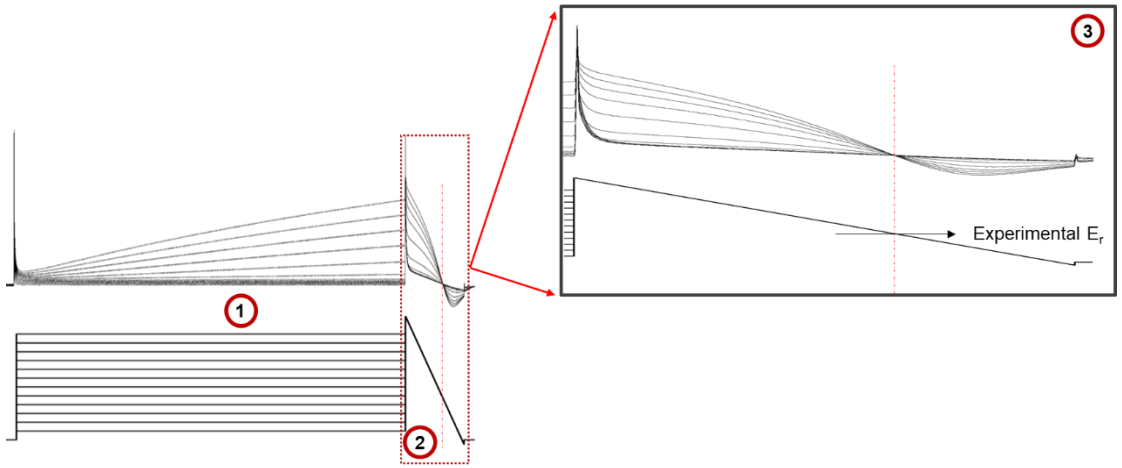


**Figure 15. Fast ramp method for estimates of reversal potential.** The fast ramp method involves two important steps: (1) voltage pulses prior to the application of the ramp, and (2) the fast voltage ramp. In (3), a magnified view of the current traces obtained after the application of the fast ramp can be observed, showing the intersection of the currents that indicates the experimental reversal potential value.

During the application of the voltage ramp, the traces elicited by the ramp cross exactly at the experimental $E_r$ **(Figure 15)**.

The demonstration of this phenomenon is explained by Ohm's law, which for membrane containing channels can be expressed as follows:

$$I = G\ (V - E_r) \qquad (Equation\ 14)$$

The total macroscopic current ($I$) equals the sum of the products between proton and leak conductances ($G$) with their respective electromotive forces ($V - E_r$) plus the capacitive current ($C\frac{dV}{dt}$):

$$I = G_{H^+}(V - E_{H^+}) + G_{leak}(V - E_{leak}) + C\frac{dV}{dt} \qquad (Equation\ 15)$$

For all current traces, the terms $G_{leak}(V - E_{leak})$ and $C\frac{dV}{dt}$ are the same. It is important to note that $G_{leak}$ emerges from possible artifacts due to not having a perfect electrical seal between the membrane patch and the recording pipette, or due to membrane damage, which allows ion permeability in a non-specific manner. However, as $G_{leak}$ does not correspond to ionic conductivity through an ion channel, its behavior is Ohmic (linear). Therefore, in the expression of Equation 13, the only term that varies with each of the applied pre-pulses corresponds to $G_{H^+}(V - E_{H^+})$. Thus, each of the current pulses prior to the fast ramp arrives with a different $P_O$, which is reflected in different amplitudes of the macroscopic current. Hence, when the rapid ramp takes the same voltage value as the experimental reversal potential, that is, $V = E_{H^+}{}^+$, the term of the macroscopic current is given by:

$$I = G_{leak}(V - E_{leak}) + C\frac{dV}{dt} \qquad (Equation\ 16)$$

This term is identical for each of the pre-pulses and, therefore, the current traces overlap, even though they have different slopes (**Figure 15**), that is:

$$I(V_i) = I(V_{i+1}) \qquad (Equation\ 17)$$

During the development and application of the protocol it is important to consider that the duration of the applied ramp depends on the deactivation time constants ($\tau_{deact}$) of the channel currents. If the applied ramp is too slow, in addition to mobilizing more protons, it can cause the decrease in applied membrane potential to close the channels before observing the crossing of the pulses, as seen in Figure 16. For Hv1 currents, both $\tau_{deact}$ and $P_O$ are temperature-dependent, pH-dependent, membrane voltage-dependent, phosphorylation-dependent, and may be affected by the presence of certain inhibitors such as divalent metals.

Thus, depending on the experimental conditions, it is recommended not only to standardize the duration of the ramp but also the voltage range it covers, with the

intention that for the entire ramp, $P_O \neq 0$.

An example of this protocol standardization applied on wild type Hv1-injected oocytes is shown in Figure 16A and B. The presented experiments were performed under conditions of ΔpH 0 ($pH_{in}$=$pH_{out}$=7.0). Here, a potential ramp of 80 ms was applied in the range of +200 mV → -200 mV **(Figure 16A)**.

It can be observed that, with the applied pulse protocol, $P_O$ reaches 0 value before the crossing of the current traces **(Figure 16 A and B)**. Three elements were taken into consideration to ensure the crossing of the current traces: (1) duration of the fast ramp, this must be fast enough to cover the voltage before the channel closes ($P_O \neq 0$); (2) range of the fast ramp: if the potential ramp reaches very negative voltages, this will favor the closing of the channels; and (3) amplitude of the pre-pulses: the pulses applied prior to the potential ramp must lead the membrane channels to a Po large enough to successfully record currents, but without inducing proton depletion. In Figure 16 C and D, the recordings were obtained considering the corrections mentioned above, shortening the duration of the ramp to 30 ms, and modifying the potential range from -100 to +190 mV. Thus, the current overlap was obtained to estimate the experimental $E_r$.

When using this protocol, a displacement in the current traces may be observed in some cases. This occurs only when there is inadequate pH control or the protocol is poorly calibrated **(Figure 16 E)**, which is an indication that the $E_r$ for protons is being affected during the experiment due to proton depletion. From the displacement of poorly calibrated recording current traces, local crossing between successive pulses can be observed **(Figure 17)**. In this way, in the representative recording of Figure 17, we can see how the reversal potential values deviate from the value predicted by the Nernst equation due to proton depletion during the pulse protocol. As expected, proton depletion increases and accumulates as the experiment develops. It is important to note that in the recording where the crossing is observed, there is no clear drop in the amplitude of the macroscopic current, so at first glance, this recording appears to be free of depletion. With the analysis of the reversal potential, we observe that it is precisely the opposite. This is clear evidence that a criterion to

obtain reliable and reproducible data  is necessary to be established when dealing with macroscopic proton currents.

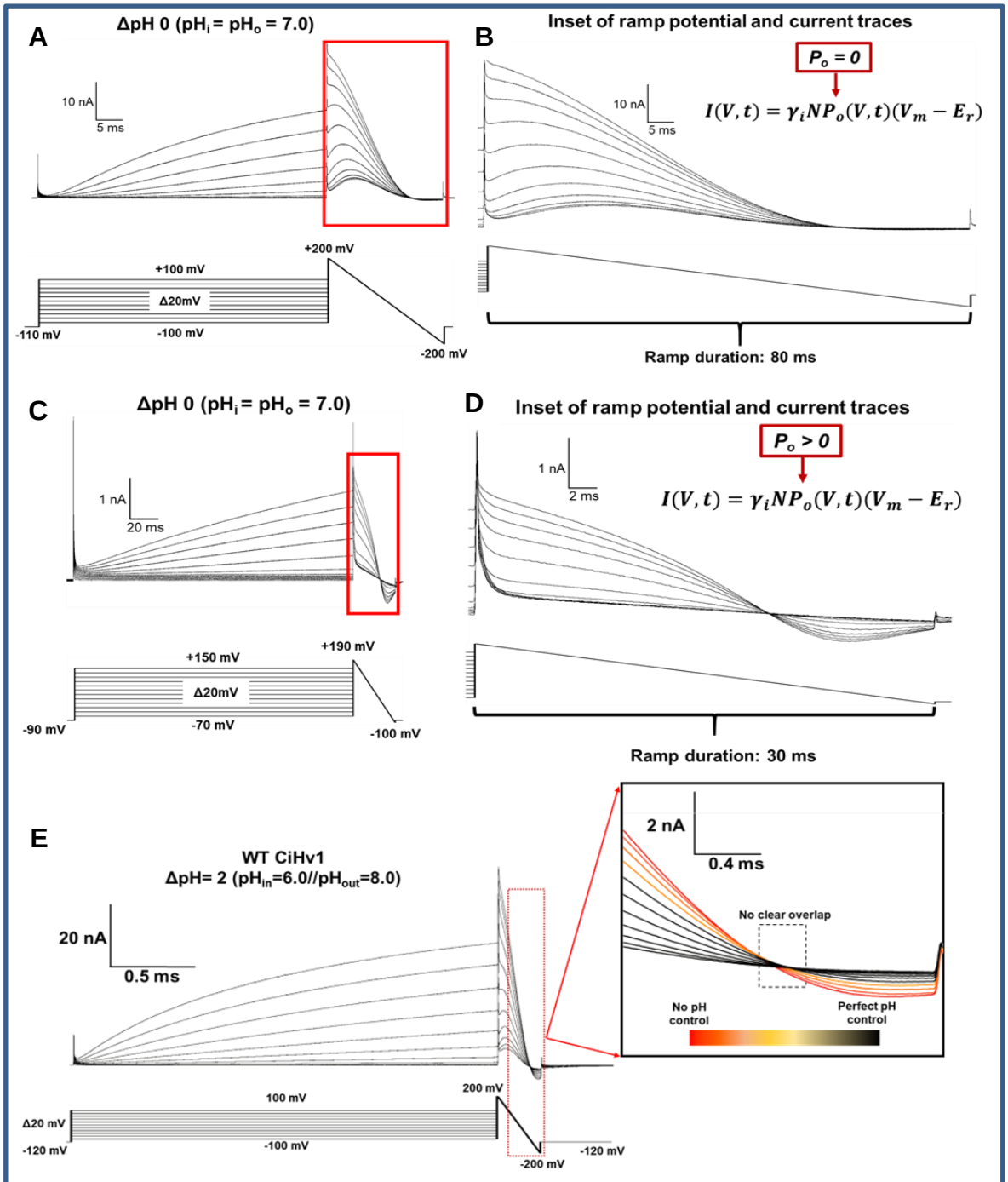


**Figure 16. Calibration of the fast ramp protocol. (A y B)** When the voltage ramp starts with low Po, the current amplitude rapidly tends to zero, making it impossible to achieve current superposition. **(C and D)** To achieve current superposition, the voltage protocol, especially the pulses before the ramp, must be adjusted according to the experimental conditions used to study the proton channel. **(E)** If the protocol is poorly calibrated and the pH conditions continue to change due to proton depletion, it becomes impossible to observe current superposition, as demonstrated in the representative recording.

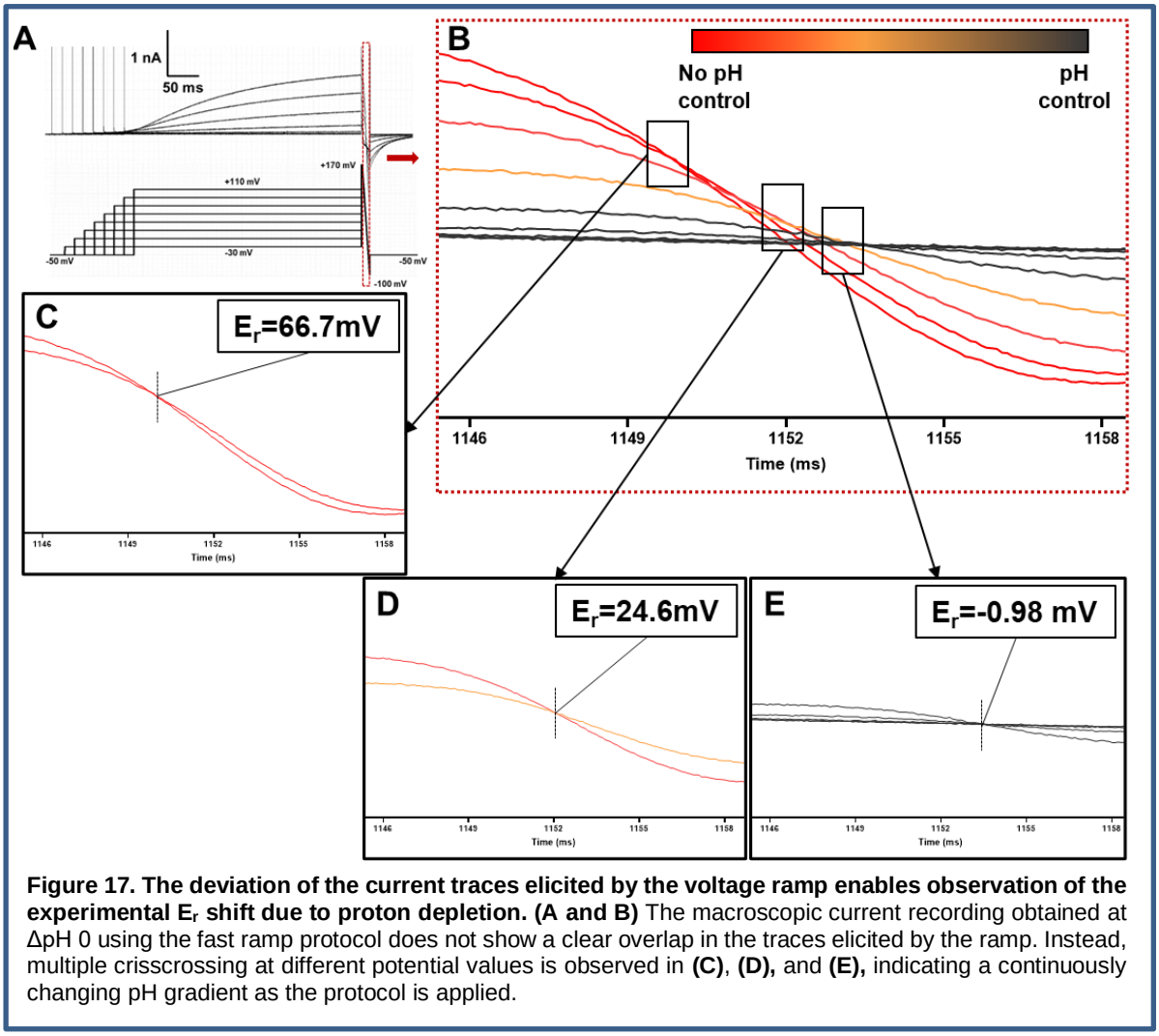


**Figure 17. The deviation of the current traces elicited by the voltage ramp enables observation of the experimental $E_r$ shift due to proton depletion. (A and B)** The macroscopic current recording obtained at ΔpH 0 using the fast ramp protocol does not show a clear overlap in the traces elicited by the ramp. Instead, multiple crisscrossing at different potential values is observed in **(C)**, **(D),** and **(E),** indicating a continuously changing pH gradient as the protocol is applied.

Taking all the above into consideration, this protocol was used before and after obtaining macroscopic proton currents as a validation criterion for the pH conditions in the experiment to determine the GV curves.

## 2) Electrophysiological Characterization of CiHv1 WT, N264E and N264R

As discussed in the Introduction, the asparagine in the S4 alpha helix of the Hv1 proton channel is highly conserved. In *C. intestinalis* (CiHv1), this corresponds to position N264. As mentioned in the Introduction, mutations directed at position N4 severely affect the conducting properties of the mouse, human and sea squirt channels (Carmona et al. 2018; Qiu et al. 2013; Randolph et al. 2016; Sakata et al. 2010). Residue N264 is located at the end of the S4 segment, facing the cytosolic entrance of the Hv1 permeation pathway, so collectively, these data suggest that it could have an interesting role in proton permeation. The following is an electrophysiological characterization to elucidate how certain mutations directed at the N264 residue modulate the conducting profile of the channel with the intention of understanding the potential role of this residue in the permeation mechanism of this protein.

### I. Study of the Macroscopic Currents and GV Curves of the CiHv1 WT Channel and the N264E and N264R Mutants

Following the methodology outlined in the previous section, we recorded macroscopic currents in CiHv1 and different mutants at position N264. A variable duration pulse protocol was used to obtain GV plots, and immediately afterwards applied a fast ramp protocol to test experimental pH conditions. Experimental $E_{H^+}$ was compared to the $E_r$ predicted by the Nernst equation, and proton depletion was assumed in cases where the two values deviated. In these cases, the data was excluded from further analysis.

Replacing asparagine by a positive residue such as arginine (N264R mutant) resulted in a poorly conducting construct **(Figure 18)**. Interestingly, this residue is homologous to the fourth arginine of the voltage sensor of the voltage-sensitive phosphatases (VSP), a protein that shares some structural similarities with Hv1 since it has four transmembrane segments, although it does not conduct ionic

currents (Okamura, Fujiwara, and Sakata 2015). As shown in Figure 18, this mutation significantly reduces the macroscopic current under the patch-clamp technique for the given experimental conditions, confirming prior findings from literature. However, when asparagine is replaced with a negatively charged amino acid, such as glutamate in the N264E mutant, a macroscopic current is obtained **(Figure 18)**.

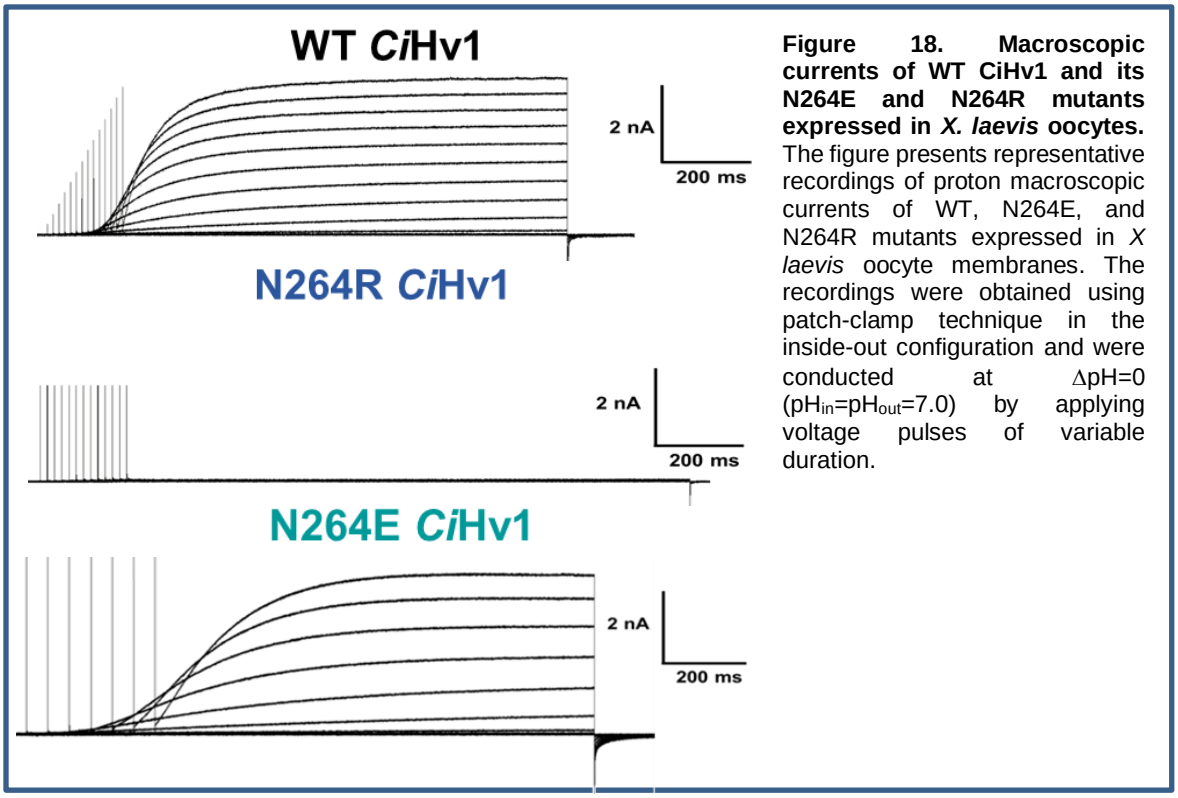


**Figure 18. Macroscopic currents of WT CiHv1 and its N264E and N264R mutants expressed in *X. laevis* oocytes.** The figure presents representative recordings of proton macroscopic currents of WT, N264E, and N264R mutants expressed in *X laevis* oocyte membranes. The recordings were obtained using patch-clamp technique in the inside-out configuration and were conducted at ΔpH=0 ($pH_{in}$=$pH_{out}$=7.0) by applying voltage pulses of variable duration.

Figure 19 displays the GV relationships of the WT CiHv1 channel and the N264E mutant. The shift of the activation curve of the N264E towards more negative voltages indicates that the channel requires less voltage to open, which is a significant finding. The mutation may impact the permeation pathway, potentially promoting the passage of protons and leading to an increase in unitary conductance (γ). To determine if this is the case, it is necessary to estimate γ and the ion selectivity of the N264E mutant and compare it to the CiHv1 values. Direct measurement of the unitary conductance (γ) of the Hv1 proton channel is impossible due to the very low γ (within the order of femtosiemens, or fS) (Cherny et al. 2003).

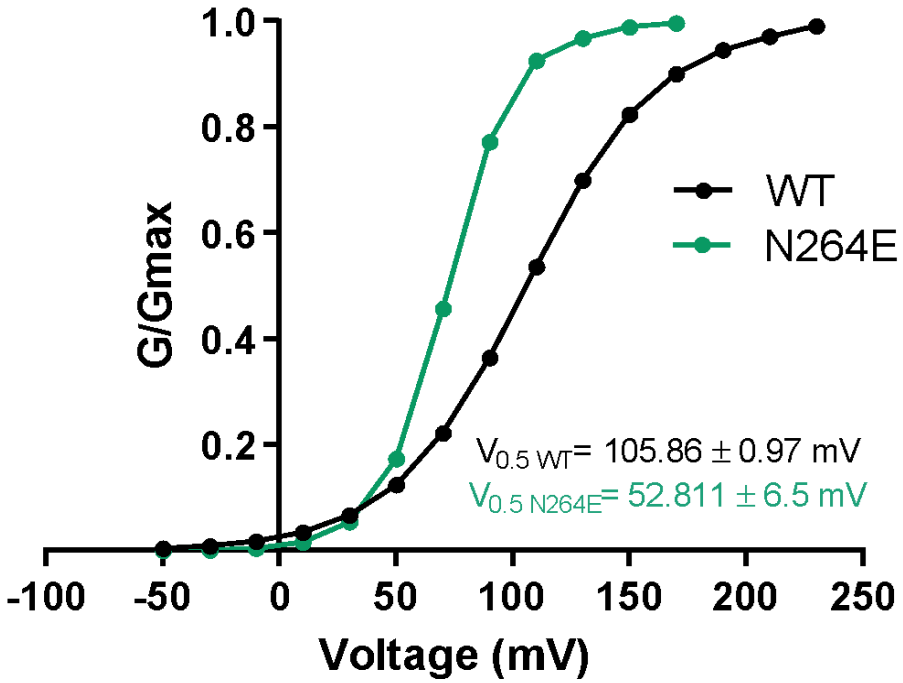


**Figure 19. Activation curves or GV relationships of macroscopic currents of WT CiHv1 and the N264E mutant expressed in *Xenopus* oocytes.** The figure presents the mean GV curves for WT CiHv1 (Black, n=6) and N264E (Green, n=3) obtained from recordings at ΔpH 0 ($pH_{in}$=$pH_{out}$=7.0). The data were fitted to a two-state Boltzmann function. The half-activation voltage ($V_{0.5}$) for WT CiHv1 channel is 105.86 ± 0.97 mV, while for the N264E mutant is 52.81 ± 6.5 mV.

To estimate the unitary conductance, the method of nonstationary noise analysis was used. This technique involves variance analysis of macroscopic current traces to mathematically obtain the single channel current value (Alvarez et al. 2002).

### II. Unitary conductance (γ) estimation of CiHv1 WT and N264E mutant

Following the nonstationary noise analysis method (Alvarez et al., 2002) (see Materials and Methods section), the conductance values of the CiHv1 WT channel and the N264E mutant were estimated. Previously, the conductance for the human proton channel has been reported with the stationary noise analysis method (see Introduction), which is in the order of fS (Cherny et al. 2003).

In this work, the γ determined for CiHv1 WT was 257 fS **(Figure 20, left panel)**. Although this value is slightly higher than the 138 fS at ΔpH 2 reported in 2003 by

DeCoursey's group (Cherny et al. 2003), our result is in the same order of magnitude. Possibly slight structural differences between the ascidian and human channels, as well as differences in the study systems (human eosinophils natively expressing the proton channel versus *Xenopus* oocytes as a heterologous expression system), explain the difference in the values of γ.

Interestingly, the N264E mutation increases γ by an order of magnitude compared to the WT channel **(Figure 20, right panel)**. This significant increase strongly suggests that the mutation at position N264 directly affects the protein permeation pathway. Unfortunately, non-stationary noise analysis is not applicable for the low-conductive N264R mutant because the amplitude of its current is too low to apply any kind of patch-clamp acquisition.

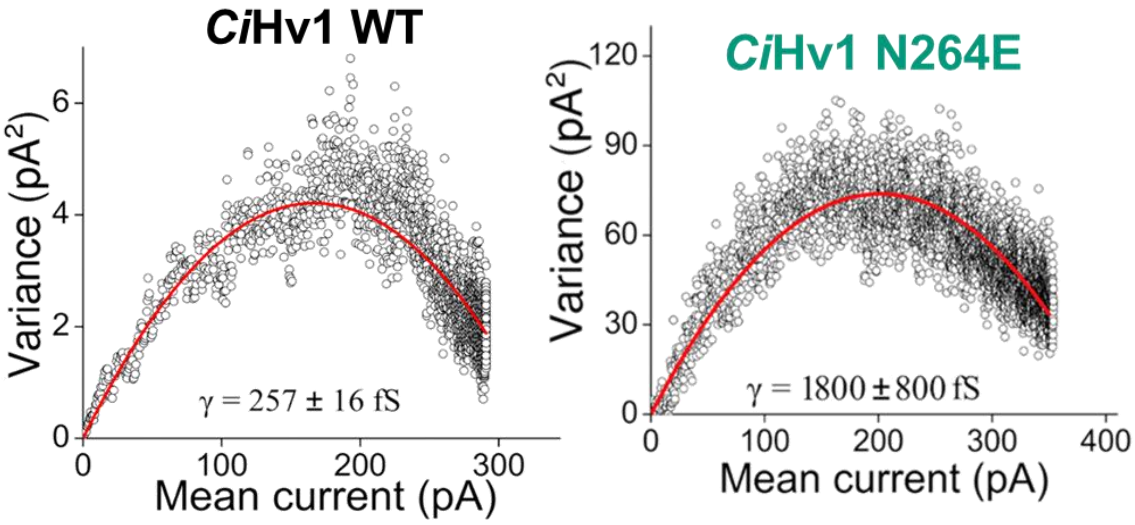


**Figure 20. The N264E mutation modulates the unitary conductance (γ) of the proton channel.** Non-stationary noise analysis was used to determine the g in WT and the N264E mutant. A square pulse was applied from -80 to +150 mV, repeated 200 times. The variance versus mean current relationship describes a parabolic shape with roots at 0,0. The fit of the initial slope provides the value of the unitary current, which can be used to estimate the value of γ. The measured g for the WT Hv1 channel is 257± 16 fS (n=3), while for the N264E mutant it is 1800 ± 800 fS (n=3).

By adding a positive charge at the position 264 of the CiHv1 channel, we observe that the resulting construct is a low-conductive channel, while the addition of a negative charge converts the channel into a superconductive protein compared to its native counterpart. Explanations for the superconductive behavior of the N264E mutant could be attributed to a loss of ionic selectivity, allowing the conduction of the other types of ionic species found in the recording solution, such as chloride or

magnesium. Although this hypothesis is unlikely due to the fact that the N264 position does not interact directly with the selectivity filter, the proton selectivity of the construct was determined in order to ensure whether the phenomenon of increased conductance is directly related to an increase in proton conductance or is an associated with a loss of ionic selectivity in the protein.

### III. Determination of the Proton Selectivity of CiHv1 WT and the N264E mutant

To determine whether the phenomenon of increased macroscopic conductance is directly related to an increase in proton conductance or is associated with a loss of ion selectivity in the protein, proton selectivity was determined by $E_r$ estimation using the fast ramp protocol. Thus, the selectivity of both proteins to different ΔpH was characterized and compared with the theoretical values predicted by the Nernst equation **(Equation 2)** for a proton selective channel **(Figure 21)**.

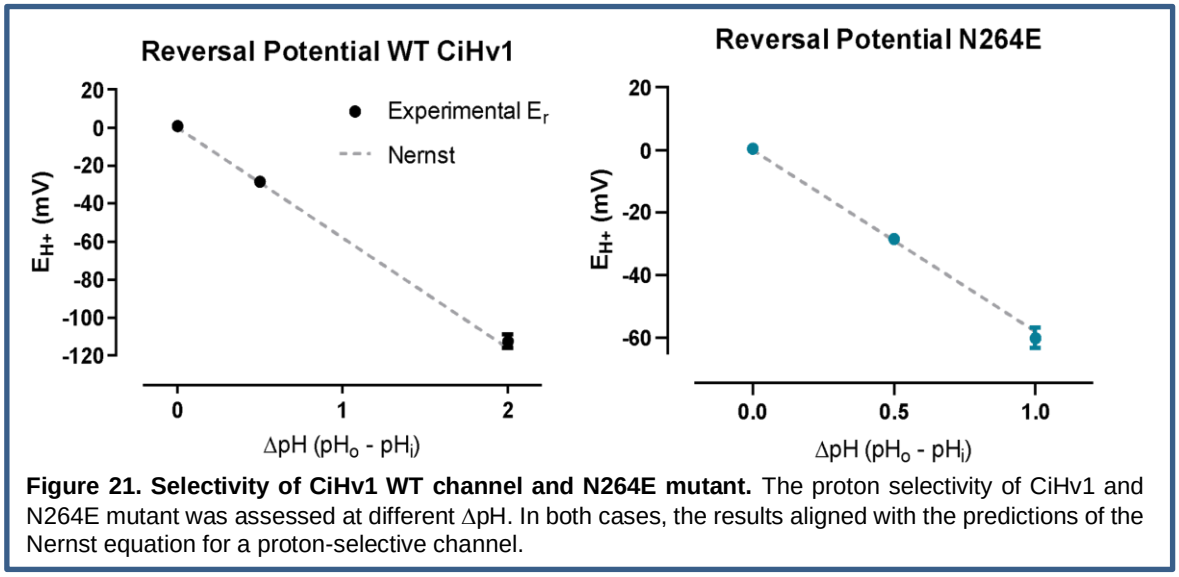


**Figure 21. Selectivity of CiHv1 WT channel and N264E mutant.** The proton selectivity of CiHv1 and N264E mutant was assessed at different ΔpH. In both cases, the results aligned with the predictions of the Nernst equation for a proton-selective channel.

The electrophysiological characterization of charge addition at position 264 suggests that the N264E mutation converts the Hv1 proton channel into a proton superconducting protein, evidencing a direct impact on the proton conduction mechanism. On the other hand, replacement of the asparagine by a positive charge in the N264R mutant resulted in a poor conducting channel. These observations raise intriguing questions about the role of the N264 position in the Hv1 proton

channel's permeation mechanism. Maybe the location of asparagine in the wild-type channel plays a role in shaping the dipole angle of water molecules near the SF on the channel's constriction zone.

The N4 position (N264 in CiHv1) of the Hv1 channel has been quite remarkable for researchers because it is a highly conserved molecular element in the channel (Musset et al., 2011; Berger and Isacoff, 2011). Conservative mutations targeted at this position, such as the ones performed by Berger and Isacoff (N4S mutant), did not alter the selective channel's behavior (Berger and Isacoff, 2011). However, consistent with our work, other previous reports have shown that adding a positive charge to this position drastically decreases channel's conduction (Qiu et al., 2013; Sakata et al., 2010; Carmona et al., 2018; Randolph et al., 2016; Ramsey et al., 2010). The interesting aspect of this position is that although it is located in the vicinity of the constriction zone, it does not have direct interaction with the selectivity filter.

It is well established that the SF and R2 or R3 (depending on the homology models constructed by different authors) interact through salt bridges, creating a stable constriction zone in the open state (Berger and Isacoff, 2011; Kulleperuma et al., 2013; Morgan et al., 2013). This interaction in the middle of the protein is crucial for proton selective conduction and charge compensation (Berger and Isacoff, 2011; Kulleperuma et al., 2013; Morgan et al., 2013).

Could the addition of a charge at this position (either positive or negative) affect and modulate the salt bridge interaction between the selectivity filter and the arginines of the voltage sensor?

By using the ΔNΔC N264R construct, Carmona and coworkers could detect and characterize the movement of the voltage sensor in CiHv1 for the first time, mainly due to the low-conductive feature conferred by the insertion of a positive charge at this position (Camona et al., 2018). Interestingly, the authors of this study reported that the OFF-gating charge exhibited immobilization or trapping, a phenomenon that also has been observed in sodium channels (Armstrong and Bezanilla, 1977). The

authors discussed that this phenomenon could be related to the addition of this charge by stabilizing the closed state of the channel, possibly through some type of electrostatic interaction, which slows down the sensor deactivation (Carmona et al., 2018). Additionally, the chimera X-ray structure revealed that the R3 is oriented towards the external region of the protein, in such a way that it can interact with the N4 (Takeshita et al., 2014).

Thus, the change in the conduction behavior of the N264 mutants could be explained by rearrangement of the interactions near the Asp-Arg interaction. However, could this be the sole explanation or additional elements are needed to be considered in proton conduction? For example, it is unknown if the water configuration at the vicinity of the constriction zone is important for proton permeation.

To answer these questions, molecular dynamics (MD) simulations were performed to evaluate the constructs and examine water configurations in the channel, paying particular attention to the channel's constriction zone and the electrostatic profiles of each construct.

## 3) Study of Water Configuration, Water Density, Surface Charge Profiles and the Asp-Arg molecular interaction by Molecular Dynamics of CiHv1 WT and N264 mutants

As mentioned in the introduction asparagines play a key role in rotating the dipole angle in aquaporins, which allows water conduction in a selective and bidirectional manner (Ozu et al. 2022). Because the mechanism of proton permeation cannot be separated from studies of water in the system, it is important to explore the potential role that N264 might have on the nature of water in the constriction zone, in addition to assessing whether the observed effects on the positive and negative modulation of conduction with the previously characterized mutants are also related to changes in the hydration and dipole angle profiles of water molecules. Understanding this could give important elements to understand the changes in the conduction properties of the channel and finally, to approach a more complete model that explains the mechanism of proton permeation in the Hv1 channel.

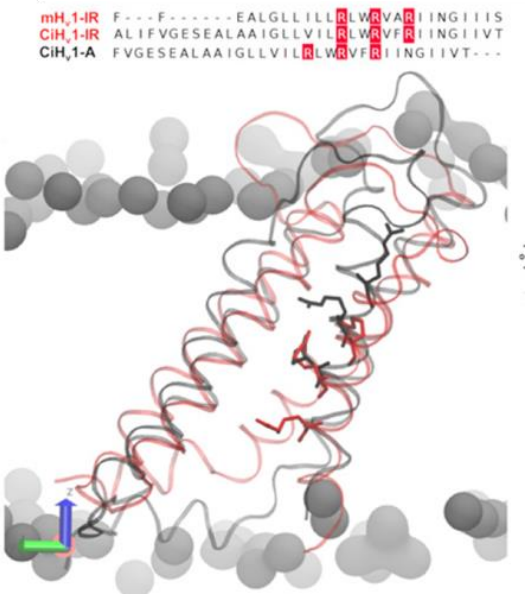


**Figure 22*. The active model of CiHv1 was built using a previously reported methodology.** A homology model of the CiHv1 channel (CiHv1-IR) in the intermediate-resting state was built using the chimeric crystal structure of the mouse Hv1 (mHv1-IR). The active model of the CiHv1 (CiHv1-A) was generated by displacing the S4 arginines in the alignments (R255, R258 and R261, highlighted in red). In the low panel, a representative snapshot from the 100 ns molecular dynamics simulation is displayed, with the S4 arginines depicted in licorice representation for both CiHv1-IR (red) and CiHv1-A (black).

****This figure was published in Carmona et al., PNAS 2021 https://doi.org/10.1073/pnas.2025556118.***

Therefore, a model of the active CiHv1, N264E and N264R channel was constructed by homology shifting the S4 alpha helix approximately 0.5 nm towards the extracellular side **(Figure 22)**, following a methodology that has been previously

used by our laboratory and others (Carmona et al. 2021; Gianti et al. 2016).

## I. Study of hydration profile and water dipole angle configuration in CiHv1 WT and the N264 mutant

The hydration profile, or water density profile, was quantified in the active channel and the mutant models by measuring the relative probability ($P/P_0$) of finding water molecules along the structure. This was achieved by defining a cylindrical pore with dimensions of 2 nm in length and 0.3 nm in diameter. Three 100 ns simulations were performed at 0 mV, and the $P/P_0$ values were averaged.

Figure 23 shows the $P/P_0$ along the structure, from the intracellular bulk (negative values on the Y-axis) towards the extracellular bulk (positive values on the Y-axis). $P/P_0$=1 is equivalent to the amount of water molecules in the bulk. It is important to note that point 0 on the Y-axis corresponds to the selectivity filter of the channel (D160 in CiHv1), and around this point, the constriction zone of the channel marked by dashed black lines can be observed. As seen in the hydration profile of CiHv1 WT, the probability of finding water decreases from the intracellular to the extracellular side, reaching a minimum in the channel's constriction zone. Then, a gradual probability increase is observed towards the extracellular side, until the bulk is reached. An important observation is that water density never reaches the zero value, indicating that a continuous chain of water molecules is formed in the permeation pathway of the WT protein in its active state, from intracellular to the extracellular bulks.

The profile observed in the N264E super proton conductor construct is quite similar to the WT, with a noticeable trend of decreasing relative probability near the selectivity filter, in the constriction zone on the extracellular side.

Undoubtedly, the profile of the poorly conductive N264R mutant stands out from the analysis, showing a very low relative probability in the constriction zone. This result is quite enlightening, as it suggests that water density may play an important role in defining a poorly or non-conductive profile.

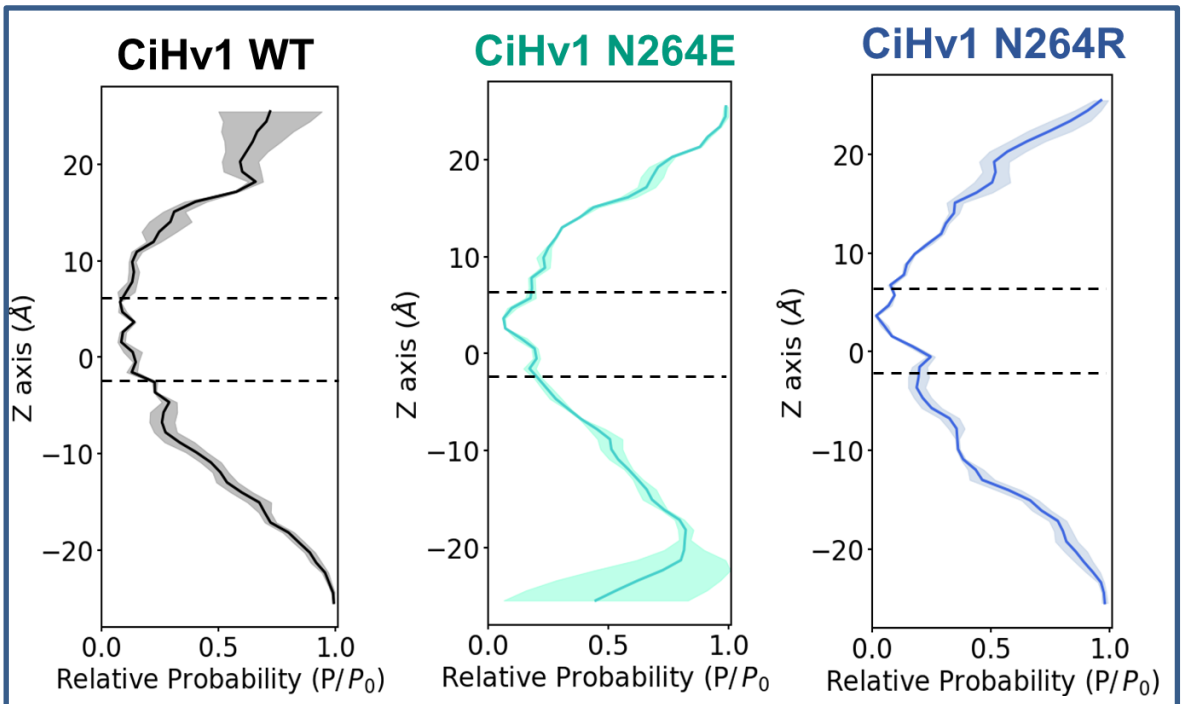


**Figure 23. Hydration profiles or water density along the defined pore for CiHv1 WT, N264E and N264R constructs in the active state at 0 mV.** The figure shows the relative probability (P/P0) of finding water molecules along the structure of the constructs in the active state at 0 mV. Different hydration profiles can be observed, particularly in the channel constriction zone, marked by dashed black lines. The ordinate axis represents the relative position of the structure along the Z-axis, with the selectivity filter residue D160 in CiHv1 serving as the reference point at position 0 Å.

As discussed in the introduction of this work, asparagines play a crucial role in water conduction in aquaporins. Specifically, the asparagines in the NPA motifs of loops B and E coordinate water molecules through H-bonds and determine its rotation in the permeation pathway. At the same time, the electrostatic profile at the NPA region creates an energy barrier for the passage of protons. In comparison, the asparagine in the S4 alpha helix of the proton channel could be affecting the configuration of the dipole angle of water molecules to enable proton conduction.

In order to answer this question, the average orientation of the water dipole angle was evaluated along the Z-axis of each construct in active state, by means of 100 ns molecular dynamics simulations at 0 mV **(Figure 24)**.

Figure 24 shows the cosine of the dipole angle along the Z-axis (cos(Θz)). In the bulk, water molecules do not have specific configurations, and since the cosine function is periodic, the average of many angle configurations is zero. As can be seen in CiHv1 WT, the water molecules at the constriction zone (near the selectivity

filter) adopt two stable configurations close to 0.5 (60° angle to the Z-axis) and -0.5 (120° angle to the Z-axis). Interestingly, for the superconductive mutant N264E, it can be observed that the angle of water molecules does not have very stable configurations and behaves similarly to water molecules in the bulk.

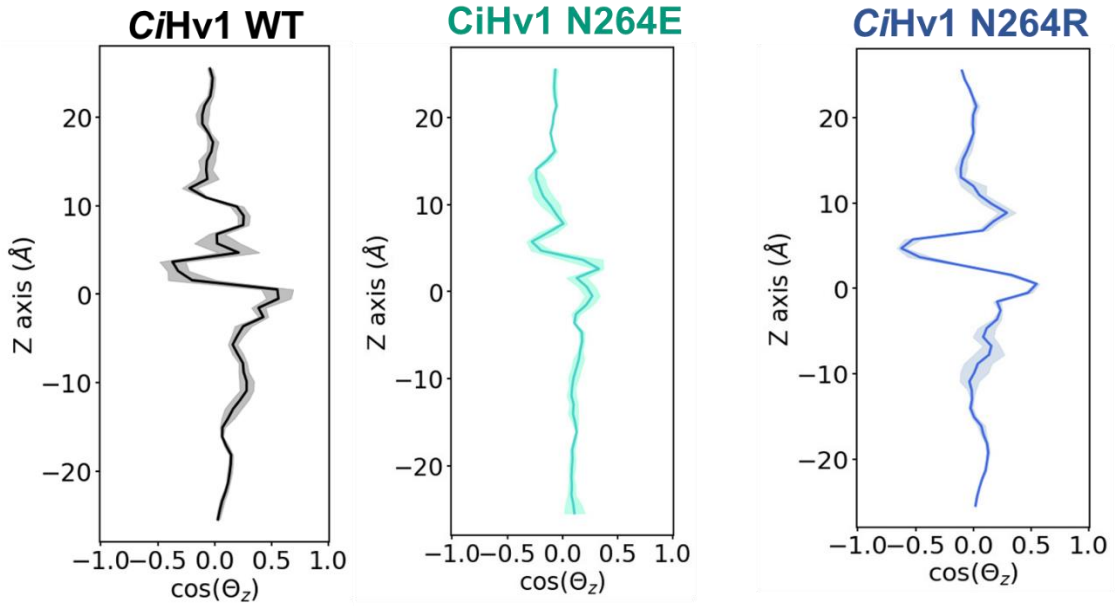


**Figure 24. Orientation of the dipole angle of water molecules along the permeation pathway in CiHv1, N264E and N264R mutants in the active state at 0 mV.** The figure displays the cosine of the angle between the water molecules and the Z-axis of the simulated protein. The average values were obtained from three simulations, each running for 100 ns, for the different constructs performed at 0 mV. The orientation of the dipole angle of water molecules changes along the structures changes in all three constructs, especially in the channel constriction zone.

The fact that water molecules behave this way in the channel's constriction zone suggests that proton conduction occurs similarly to bulk water, thus explaining its high γ value.

If we focus on N264R, we can observe a slight difference in the angle compared to the WT construct. This particular configuration could potentially create a higher energy barrier for the passage of protons, especially the configuration of the water molecules in the constriction zone on the extracellular side.

The water profiles reveal interesting information that can be correlated with the conduction profiles recorded for the constructs in electrophysiology. However, another profile that should be explored to broaden our perspectives is the electrostatic profile of the WT protein and its comparison with both mutants. as both

involve charge additions. Therefore, molecular dynamics simulations were also conducted to study the electrostatic profiles obtained after 100 ns simulations at 0 mV.

## II. The surface electrostatic profile of CiHv1 WT, N264E and N264R

The charge insertion could affect the proton permeation pathway of the protein, having a significant impact on the observed proton conduction. In Figure 25, we can observe a “smooth” negative electrostatic potential along the N264E mutant, presenting few electrostatic energy barriers for the flow of positively charged particles like protons. This profile could even suggest a possible proton permeation pathway for the Hv1 channel. On the other hand, the N264R mutant exhibits a positive density near the constriction site, which can even induce polarization of the structure. This not only creates a local positive density, causing the repulsion of protons, but also the generated protein polarization could explain the configuration of the water dipole orientation.

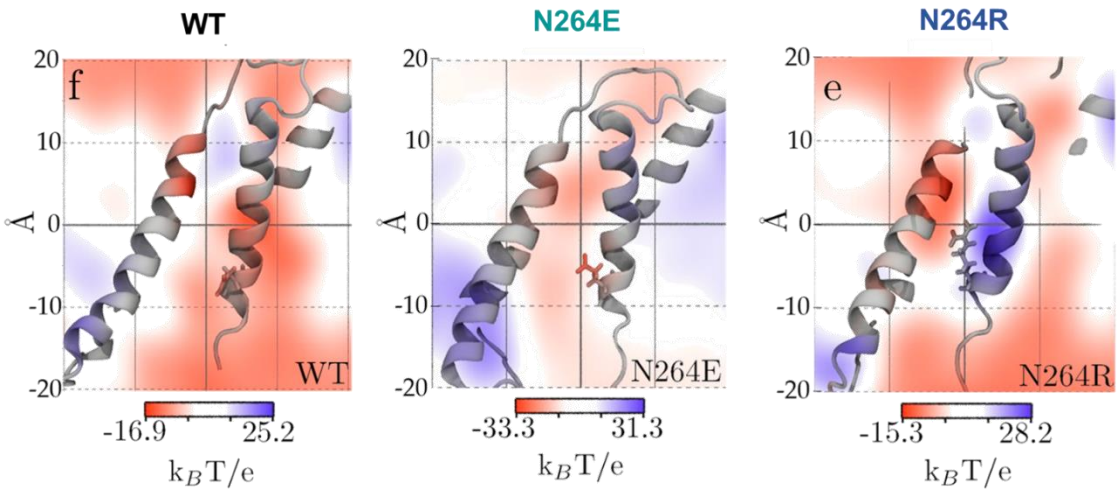


**Figure 25. Surface electrostatic profile of CiHv1 WT, N264E and N264R in the active state at 0 mV.** The figure shows the variations in the surface electrostatic profile, represented by a color map where red indicates negative charge density and blue indicates positive charge density.

It can be observed that when a positive charge is provided (like in the N264R mutant) the electrostatic map of the channel changes with respect to the WT, showing the formation of a dramatic polarization between the S4 transmembrane segment that contains the 4 arginine residues and the S1 transmembrane segment where the filter

selectivity is located. The addition of the positive charge in the position 264 could be affecting the interaction between Asp-Arg in the constriction zone. To assess that possibility, an examination of the distances between SF-R2 and SF-R3 was explored in the simulations.

### III. Examination of the Asp-Arg interaction in CiHv1 WT, N264R and N264R

It is widely described in the literature that the formation of the Asp-Arg salt bridge interaction in the middle of the channel is crucial for proton selectivity and conduction (see *Introduction, Chapter 3, "The Selectivity Filter and the Channel's Permeation Pathway"* section).

This interaction was evaluated by means of MD simulations in the active models of each construct by measuring the distances between the studied residues (SF, R2 and R3). The distances computed are shown in Figure 26. The predictions suggest that R2 maintains a shorter distance to the selectivity filter compared to R3 in the native protein. Distances of interactions serve as a strength indicator of the attraction between them. Therefore, salt bridge interactions are characterized by having an approximate distance of 4 Å , which is consistent with the literature (Sinha et al., 2007). In our models, the constriction zone would correspond to the DF-R2 salt bridge interaction. Interestingly, the N264R mutation stabilized the interaction between R2 and R3 with the selectivity filter, suggesting a structural change in the interactions at the constriction zone, promoting a triad of salt bridges. This could explain the observations in the hydration profiles, where the decrease in the distance between the second and third arginine and aspartate hinders the passage of water, as well stabilizing certain configurations that impair proton conduction, and also generating a strong electrostatic barrier that promote a repulsive force for proton movement. Similarly, we can explain how the introduction of a negative charge, such as glutamate, would have the opposite effect, destabilizing the salt-bridge interaction between the SF and R3 **(Figure 26)**.

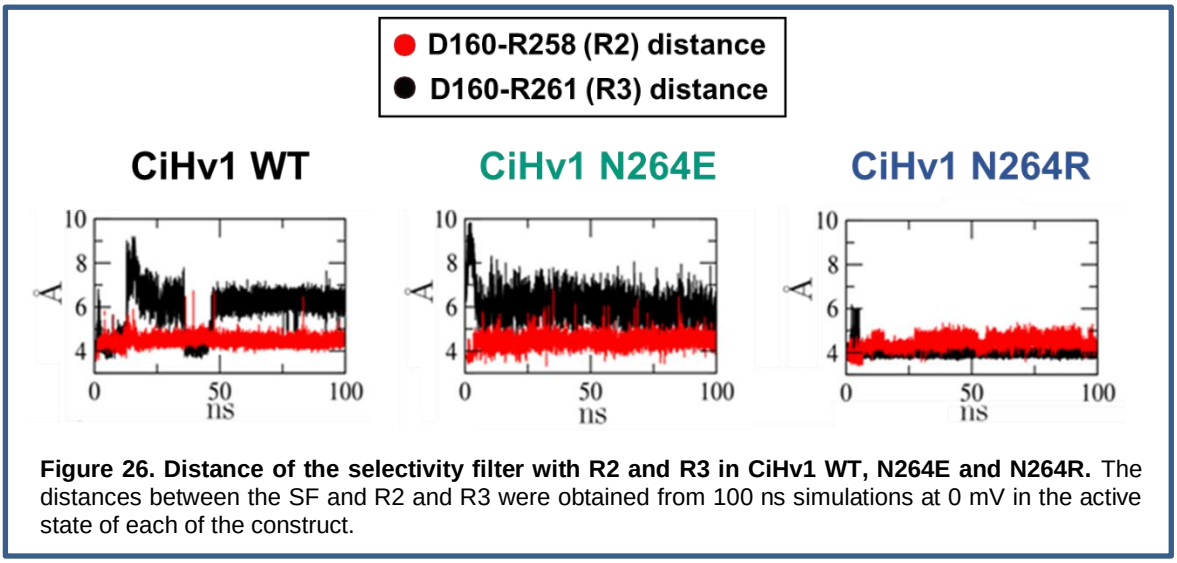


**Figure 26. Distance of the selectivity filter with R2 and R3 in CiHv1 WT, N264E and N264R.** The distances between the SF and R2 and R3 were obtained from 100 ns simulations at 0 mV in the active state of each of the construct.

Although there is controversy regarding which of the arginines (R2 or R3) of the sensor forms the interaction with the selectivity filter in the open state, the crystal structure of the mHv1cc suggests that the salt bridge interaction in the *Intermediate Resting* state occurs between R1 and R2 (Takeshita et al., 2014). This is interesting because our computational predictions support the idea that the addition of a positive charge, at least in the N264R mutant, would promote salt bridge interactions between SF-R2 and SF-R3 simultaneously, possibly originating from electrostatic repulsion exerted over R3. Thus, this mutation would be mediating a restructuring of the constriction zone, which can partially explain the nonconductive nature and the water profiles predicted by MD. This can also partially explain some previously reported data in the literature, such as the charge trapping observed in the ΔNΔC N264R mutant (Carmona et al., 2018). While these observations are compelling, the rearrangement of the constriction zone observed in the superconductive N264E mutant solely cannot explain the observed changes in the electrophysiological recordings. However, it makes sense when considering the hydration profiles and the dipole angle configuration of water molecules. Thus, the proton permeation in the Hv1 channel may be supported by two components, at least: the electrostatic nature of the constriction zone, and the nature of water in the vicinity of the constriction zone in terms of hydration and molecular dipole angles.

Due to the fact that the permeation pathway of the proton channel in its open state

has not been structurally resolved yet, the presence and absence of water molecules and their configurations can only be computationally simulated. However, the chimera structure suggests the presence of a cavity that houses water molecules near the selectivity filter (Takeshita et al., 2014). Since computationally simulated hydration profiles show a continuous presence of water in the active state of the protein, the proton channel could be conducting water, or it could contain immobilized water as a structural feature of the protein.

Moreover, homology models of some research groups agree with the idea of hydration sites spanning the entire proton permeation pathway in the active state (Ramsey et al., 2010; Gianti et al., 2016; Carmona et al., 2021). If the permeation pathway of the channel is entirely hydrated, water fluxes could be observed.

Experimentally, we can determine if the protein increases the osmotic permeability of biological membranes using strategies implemented to study aquaporins to assess how the osmotic permeability of cellular membranes or tissues changes in front of osmotic variations.

## 4) Study of water transport in *Xenopus* oocytes injected with CiHv1 WT and the mutants N264E and N264R

To evaluate whether the CiHv1 proton channel allows the movement of water molecules through its permeation pathway, or whether they are immobilized and form part of the structural constriction zone of the channel, then osmotic experiments were performed with wild type CiHv1, or mutants N264E-, or N264R-injected oocytes. The oocytes were subjected to a 160 mOsm $Kg_w^{-1}$ hypoosmotic gradient by using a 1/5 dilution of ND96 calibrated to pH 9.4, to establish a ΔpH 2 (assuming an intracellular oocyte pH of 7.4), with the intention of promoting the opening of the channels expressed in the oocyte membrane. The osmotic response recorded in a typical experiment is shown in **Figure 27**.

Results show a volume increase in all oocytes injected with Hv1 (in spite of the mutation). However, the initial slope of the volume change is higher in wild type CiHv1- and N264E-injected oocytes.

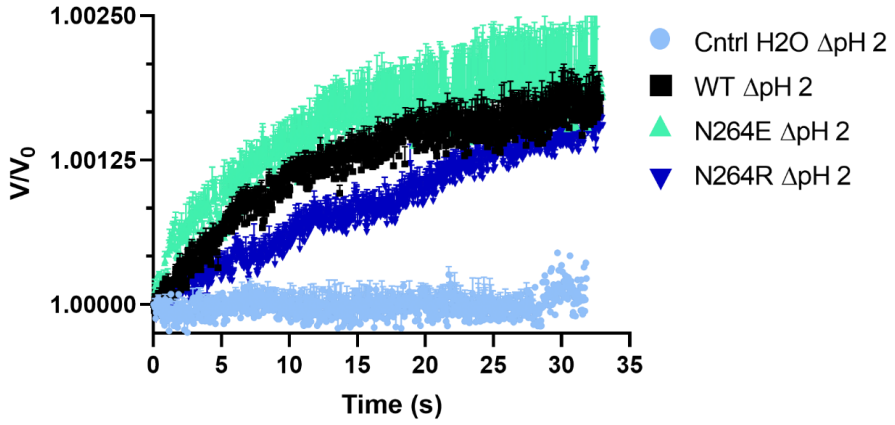


**Figure 27. $V/V_0$ over time following a hypoosmotic shock in oocytes injected with CiHv1, N264E and N264R.** The figure presents the mean curves obtained for the volume change in response to an osmotic shock of Δ160 mOsm.$Kg_w^{-1}$ at ΔpH 2 for oocytes injected with water (cyan, n=3), CiHv1 WT (black, n=4), N264E (green, n=3) and N264R (blue, n=3).

The analysis of these results shows significant differences in $P_f$ values wild type and mutants of CiHv1 against water-injected oocytes (**Figure 28**). This suggests that if CiHv1 channels are open, then a tiny water flux can occur in the presence of an

osmotic gradient, suggesting that Hv1 can transport water. Furthermore, results show that the water transport through Hv1 is impaired in the N264R mutant but not in the N264E mutant. This suggests that the positive charge at position 264 is detrimental for water transport.

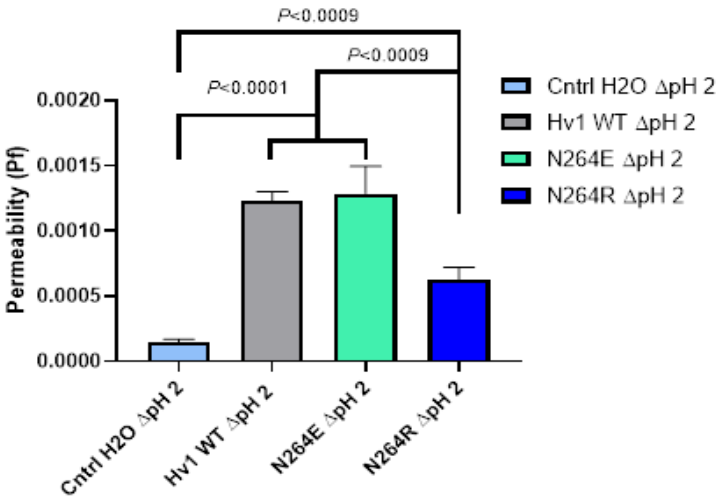


**Figure 28. $P_f$ of oocyte membranes injected with CiHv1 WT, N264E and N264R.** The osmotic permeability obtained from the initial slope fitting of oocyte volume changes is shown in the figure. The $P_f$ values were: $1.5x10^{-4} \pm 2.5x10^{-5}$ cm $s^{-1}$ for Control $H_2O$ (cyan), $1.2 \times 10^{-3} \pm 6.9 \times 10^{-6}$ cm $s^{-1}$ for Hv1 WT (gray), $1.2 \times 10^{-3} \pm 2.0 \times 10^{-4}$ cm $s^{-1}$ for N264E (green) and $6.3 \times 10^{-4} \pm 9.1 \times 10^{-5}$ cm $s^{-1}$ for N264R (blue). Data were presented as mean ± SEM. P<0.05 was considered statistically significant (Student's t-test).

Interestingly, the observed $P_f$ values are in accordance with the hydration profiles observed in the molecular dynamic simulations (See Figure 23). As mentioned in the precedent paragraph, the water permeability is significantly lower in the non-conducting N264R-mutant than in the native CiHv1 and the superconductive N264E-mutant. Therefore, the position N264 would have an important role in the structural organization of water in the proton pathway, which would impact on both the low water permeability of the channel and the scaffolding of the proton permeation pathway. Altogether, the experimental and simulation data suggest that the active channel configuration favors both the water movement in simultaneous with proton conduction, through the same pathway.

The mechanism by which protons permeate through the Hv1 channel has been subject of intense debate, mainly due to the unconventional structure of this protein.

Hv1 lacks the typical pore domain found in most voltage activated ion channels. Here, we provide key elements to unlock the mysteries of proton conduction: the hydration profile, the dipole angles configuration, the modulation of the electrostatic profile by the position of amino acid 264 in *Ciona intestinalis*, and the capacity of the proton channel to transport water.

Previous reports show that substitution N4R impairs the channel conductance (Sakata et al., PNAS 2010, Ramsey et al., B. J Elsevier 2014, Randolph et al., Elife 2016, Qiu et al., Neuron 2013, Carmona et al., PNAS 2018). Previously, our group reported that the gating currents observed with ΔNΔC N264R mutant of CiHv1 suffer trapping of the OFF component (Carmona et al., PNAS 2018). Then, the substitution of a neutral charge by a positive one at position 264 modifies the electrostatic environment inside the channel but also involves a conformational rearrangement of the protein. Here, we tested this idea by means of electrophysiological measurements and found that charge additions in the N264 position (Glutamate and Arginine) dramatically affected the conductive properties. The N264R mutation has such a low conductance that it is impossible to perform a non-stationary noise analysis protocol due to the small amplitude of the evoked current, compared to the wild type. On the other hand, $\gamma$ is significantly increased in the N264E mutant, in which the charge value is negative. Furthermore, this mutation alters the balance between open-closed states, shifting the GV curve to the left and showing $V_{0.5}$ = 52.811± 6.5 mV. One of the important results found in this work is that alterations in the N264 position affect the conductance properties but do not alter the selectivity of the channel. Thus, adding charges at this position helps us to unravel some properties of the proton transport mechanism.

Water occupancy in our active WT and N264E models spans the entire proton permeation pathway. In contrast, in the low conductive construct a water occupancy close to zero is observed in the vicinity of the selectivity filter (SF). Possibly, this is a result of the repulsion generated towards the R3 position that promotes de SF-R3 salt bridge interaction and consequently stretching the permeation pathway. This could disrupt a hypothetical water continuum and impairs proton conduction.

The data presented in this study allow for the addition of a new variable to the proton permeation mechanism: the water configuration in the constriction zone of the channel. For the first time, a change in membrane permeability coefficient was reported in oocytes injected with Hv1. Further research should be conducted to explore whether proton transport is accompanied by water flow and if osmotic changes favor channel conduction.

# Conclusions

The molecular mechanism by which proton permeation occurs in voltage-gated proton (Hv1) channels has been a topic of controversy, primarily due to the lack of an open structure. Consequently, all strategies aimed at determining the molecular elements governing this process have been carried out through mutagenesis studies and electrophysiological characterizations, complemented with computational predictions with homology models and Molecular Dynamics simulations. Thus, studies and reports have succeeded in identifying important elements in the protein conduction, albeit with some differences in the proposed models, precisely due to the lack of a structural template for the open protein.

The data from this work as a whole, provide a new perspective on the nature of water molecules in the protein, with particular attention to their nature around the selectivity filter and constriction zone. To achieve this, we relate changes in conductive properties with predictions of hydration profiles and channel dipole angle configuration by specifically mutating the N264 site of the CiHv1 channel.

A quantitative method was established as a criterion to assess proton depletion and enable a rigorous electrophysiological characterization of the CiHv1 channel and the N264R and N264E mutants. Through this characterization, it was observed that the addition of a positive charge converts the protein into a poorly conducting proton channel. Thus, with molecular dynamics predictions, we relate these conductive behaviors, evaluated by patch-clamp, with the hydration profile and dipole angle orientation.

We observed that mutations targeting the N264 site reconfigure the interactions between the selectivity filter and the sensor's arginines, leading to a change in the conduction properties. This structural reconfiguration modifies the probability of encountering water molecules, as well as the dipole angle orientation of the molecules in the constriction zone. Thus, mutations targeting N264 provide a better understanding of the channel's transport mechanism.

Based on the results of this work, we propose that proton transport has two components: an electrostatic effect and the nature of water in the channel's constriction zone. Additionally, hydration profiles dismiss the model proposing a

dehydrated zone in the channel's constriction zone. A dry region along the proton permeation pathway could be associated with a poorly conducting proton profile. The most conductive mutant exhibits an electrostatic profile that favors the movement of positive charge ($H^+$), but also has a favorable profile for water transport. Finally, we observed that Hv1-injected *Xenopus laevis* oocytes exhibit an increased osmotic permeability coefficient, suggesting that, although at a very low rate, this protein may also permeate water. These last data could change the entire paradigm of the proton conduction mechanism, although further studies are needed to test this hypothesis.

# References


Agmon, Noam. 1995. 'The Grotthuss Mechanism'. *Chemical Physics Letters* 244(5–6):456–62. doi: 10.1016/0009-2614(95)00905-J.

Alvarez, Osvaldo, Karen Castillo, Emerson Carmona, Carlos Gonzalez, and Ramon Latorre. 2019. 'Methods for Investigating TRP Channel Gating'. Pp. 167–85 in *Methods in Molecular Biology*. Vol. 1987. Humana Press Inc.

Alvarez, Osvaldo, Carlos Gonzalez, and Ramon Latorre. 2002. 'Counting Channels: A Tutorial Guide on Ion Channel Fluctuation Analysis'. *American Journal of Physiology - Advances in Physiology Education* 26(1–4):327–41. doi: 10.1152/advan.00006.2002.

Alvear-Arias, Juan J., Christian Carrillo, Javiera Paz Villar, Richard Garcia-Betancourt, Antonio Pe~ Na-Pichicoi, Audry Fernandez, Miguel Fernandez, Emerson M. Carmona, Amaury Pupo, Alan Neely, Osvaldo Alvarez, Jose Garate, Ector Barajas-Martinez, H. Peter Larsson, Ang Elica Lopez-Rodriguez, Ramon Latorre, and Carlos Gonzalez. 2022. 'Expression of H v 1 Proton Channels in Myeloid-Derived Suppressor Cells (MDSC) and Its Potential Role in T Cell Regulation'. doi: 10.1073/pnas.

Bada Juarez, Juan F., Peter J. Judge, Suliman Adam, Danny Axford, Javier Vinals, James Birch, Tristan O. C. Kwan, Kin Kuan Hoi, Hsin Yung Yen, Anthony Vial, Pierre Emmanuel Milhiet, Carol V. Robinson, Igor Schapiro, Isabel Moraes, and Anthony Watts. 2021. 'Structures of the Archaerhodopsin-3 Transporter Reveal That Disordering of Internal Water Networks Underpins Receptor Sensitization'. *Nature Communications* 12(1):1–10. doi: 10.1038/s41467-020-20596-0.

Bayrhuber, Monika, Innokentiy Maslennikov, Witek Kwiatkowski, Alexander Sobol, Christoph Wierschem, Cédric Eichmann, Lukas Frey, and Roland Riek. 2019. 'Nuclear Magnetic Resonance Solution Structure and Functional Behavior of the Human Proton Channel'. *Biochemistry* 58(39):4017–27. doi: 10.1021/acs.biochem.9b00471.

Berger, Thomas K., and Ehud Y. Isacoff. 2011. 'The Pore of the Voltage-Gated Proton Channel'. *Neuron* 72(6):991–1000. doi: 10.1016/j.neuron.2011.11.014.

Bezanilla, Francisco. 2018. 'Gating Currents'. *Journal of General Physiology* 150(7):911–32. doi: 10.1085/jgp.201812090.

Brini, Emiliano, Christopher J. Fennell, Marivi Fernandez-Serra, Barbara Hribar-Lee, Miha Lukšič, and Ken A. Dill. 2017. 'How Water's Properties Are Encoded in Its Molecular Structure and Energies'. *Chemical Reviews* 117(19):12385–414. doi: 10.1021/acs.chemrev.7b00259.

Buch-Pedersen, M. J., B. P. Pedersen, B. Veierskov, P. Nissen, and M. G. Palmgren. 2009. 'Protons and How They Are Transported by Proton Pumps'. *Pflugers Archiv European Journal of Physiology* 457(3):573–79.

Carmona, Emerson M., Miguel Fernandez, Juan J. Alvear-Arias, Alan Neely, H. Pete Larsson, Osvaldo Alvarez, Jose Antonio Garate, Ramon Latorre, and Carlos Gonzalez. 2021. 'The Voltage Sensor Is Responsible for ΔpH Dependence in Hv1 Channels'. *Proceedings of the National Academy of Sciences of the United States of America* 118(19):1–7. doi: 10.1073/pnas.2025556118.

Carmona, Emerson M., H. Peter Larsson, Alan Neely, Osvaldo Alvarez, Ramon Latorre, and Carlos Gonzalez. 2018. 'Gating Charge Displacement in a Monomeric Voltage-Gated Proton (Hv1) Channel'. *Proceedings of the National Academy of Sciences of the United States of America* 115(37):9240–45. doi: 10.1073/pnas.1809705115.

Cherny, Vladimir V, V. S. Markin, and Thomas E. DeCoursey. 1995. 'The Voltage-Activated Hydrogen Ion Conductance in Rat Alveolar Epithelial Cells Is Determined by the PH Gradient.' *The Journal of General Physiology* 105(6):861–96. doi: doi: 10.1085/jgp.105.6.861.

Cherny, Vladimir V, Ricardo Murphy, Valerij Sokolov, Richard a Levis, and Thomas E.

DeCoursey. 2003. ‘Properties of Single Voltage-Gated Proton Channels in Human Eosinophils Estimated by Noise Analysis and by Direct Measurement.’ *The Journal of General Physiology* 121(6):615–28. doi: 10.1085/jgp.200308813.
Covalt, James C., Melinda Roy, and Patricia A. Jennings. 2001. ‘Core and Surface Mutations Affect Folding Kinetics, Stability and Cooperativity in IL-1β: Does Alteration in Buried Water Play a Role?’ *Journal of Molecular Biology* 307(2):657–69. doi: 10.1006/jmbi.2001.4482.
DeCoursey, T. E., and V. V. Cherny. 1994. ‘Voltage-Activated Hydrogen Ion Currents’. *The Journal of Membrane Biology* 141(3):203–23. doi: 10.1007/BF00235130.
DeCoursey, Thomas E., and Vladimir V. Cherny. 1996. ‘Effects of Buffer Concentration on Voltage-Gated H+ Currents: Does Diffusion Limit the Conductance?’ *Biophysical Journal* 71(1):182–93. doi: 10.1016/S0006-3495(96)79215-9.
De-la-Rosa, Víctor, Esteban Suárez-Delgado, Gisela E. Rangel-Yescas, and León D. Islas. 2016. ‘Currents through Hv1 Channels Deplete Protons in Their Vicinity’. *The Journal of General Physiology* 147(2):127–36. doi: 10.1085/jgp.201511496.
Dudev, Todor, Boris Musset, Deri Morgan, Vladimir V Cherny, Susan M. E. Smith, Karine Mazmanian, Thomas E. DeCoursey, and Carmay Lim. 2015. ‘Selectivity Mechanism of the Voltage-Gated Proton Channel, HV1.’ *Scientific Reports* 5(April):10320. doi: 10.1038/srep10320.
Eigen, M. 1964. ‘Proton Transfer, Acid-Base Catalysis, and Enzymatic Hydrolysis. Part I: ELEMENTARY PROCESSES’. *Angewandte Chemie International Edition in English* 3(1):1–19. doi: 10.1002/anie.196400011.
Garczarek, Florian, Leonid S. Brown, Janos K. Lanyi, and Klaus Gerwert. 2005. *Proton Binding within a Membrane Protein by a Protonated Water Cluster*.
Gianti, Eleonora, Lucie Delemotte, Michael L. Klein, and Vincenzo Carnevale. 2016. ‘On the Role of Water Density Fluctuations in the Inhibition of a Proton Channel’. *Proceedings of the National Academy of Sciences of the United States of America* 113(52):E8359–68. doi: 10.1073/pnas.1609964114.
Gonzalez, Carlos, Hans P. Koch, Ben M. Drum, and H. Peter Larsson. 2010. ‘Strong Cooperativity between Subunits in Voltage-Gated Proton Channels.’ *Nature Structural & Molecular Biology* 17(1):51–56. doi: 10.1038/nsmb.1739.
Gonzalez, Carlos, Santiago Rebolledo, Marta E. Perez, and H. Peter Larsson. 2013. ‘Molecular Mechanism of Voltage Sensing in Voltage-Gated Proton Channels’. *The Journal of General Physiology* 141(3):275–85. doi: 10.1085/jgp.201210857.
de Grotthuss, C. J. T. 2006. ‘Memoir on the Decomposition of Water and of the Bodies That It Holds in Solution by Means of Galvanic Electricity.1805. (Translated from French)’. *Biochimica et Biophysica Acta - Bioenergetics* 1757(8):871–75. doi: 10.1016/j.bbabio.2006.07.004.
Hille, Bertil. 2001. ‘Ion Channel Excitable Membranes’. *Sunderland Massachusetts USA* 1–37.
Hong, Liang, Iris H. Kim, and Francesco Tombola. 2014. ‘Molecular Determinants of Hv1 Proton Channel Inhibition by Guanidine Derivatives’. *Proceedings of the National Academy of Sciences* 111(27):9971–76. doi: 10.1073/pnas.1324012111.
Hong, Liang, Medha Pathak, Iris H. Kim, Dennis Ta, and Francesco Tombola. 2013. ‘Voltage-Sensing Domain of Voltage-Gated Proton Channel Hv1 Shares Mechanism of Block with Pore Domains’. 77(2):1–20. doi: 10.1158/2326-6066.CIR-13-0034.PD-L1.
Koch, Hans P., Tatsuki Kurokawa, Yoshifumi Okochi, Mari Sasaki, Yasushi Okamura, and H. Peter Larsson. 2008. ‘Multimeric Nature of Voltage-Gated Proton Channels.’ *Proceedings of the National Academy of Sciences of the United States of America* 105(26):9111–16. doi: 10.1073/pnas.0801553105.
Kulleperuma, Kethika, Susan M. E. Smith, Deri Morgan, Boris Musset, John Holyoake, Nilmadhab Chakrabarti, Vladimir V. Cherny, Thomas E. DeCoursey, and Régis Pomès.

2013. ‘Construction and Validation of a Homology Model of the Human Voltage-Gated Proton Channel HHv1’. *Journal of General Physiology* 141(4):445–65. doi: 10.1085/jgp.201210856.
Levy, Yaakov, and José Onuchic. 2004. ‘Water and Proteins: A Love- Hate Relationship’. *Proceedings of the National Academy of Sciences* 101(10):3325–26.
Mathias, Gerald, and Dominik Marx. 2007. *Structures and Spectral Signatures of Protonated Water Networks in Bacteriorhodopsin*.
Matthews, Brian W., and Lijun Liu. 2009b. ‘A Review about Nothing: Are Apolar Cavities in Proteins Really Empty?’ *Protein Science* 18(3):494–502.
Morgan, Deri, Boris Musset, Kethika Kulleperuma, Susan M. E. Smith, Sindhu Rajan, Vladimir V. Cherny, Régis Pomès, and Thomas E. DeCoursey. 2013. ‘Peregrination of the Selectivity Filter Delineates the Pore of the Human: Voltage-Gated Proton Channel HHv1’. *Journal of General Physiology* 142(6):625–40. doi: 10.1085/jgp.201311045.
Musset, Boris, Susan M. E. Smith, Sindhu Rajan, Deri Morgan, Vladmir V. Cherny, and Thomas E. Decoursey. 2011. ‘Aspartate112 Is the Selectivity Filter of the Human Voltage Gated Proton’. *Nature* 480(7376):273–77. doi: 10.1038/nature10557.
Neher, E., and B. Sakmann. 1992. ‘The Patch Clamp Technique’. *Sci.Am.* 266(3):44–51.
Ozu, Marcelo, Juan José Alvear-Arias, Miguel Fernandez, Agustín Caviglia, Antonio Peña-Pichicoi, Christian Carrillo, Emerson Carmona, Anselmo Otero-Gonzalez, José Antonio Garate, Gabriela Amodeo, and Carlos Gonzalez. 2022. ‘Aquaporin Gating: A New Twist to Unravel Permeation through Water Channels’. *International Journal of Molecular Sciences* 23(20).
Ozu, Marcelo, Luciano Galizia, Cynthia Acuña, and Gabriela Amodeo. 2018. ‘Aquaporins: More than Functional Monomers in a Tetrameric Arrangement’. *Cells* 7(11).
Papoian, Garegin A., Johan Ulander, Michael P. Eastwood, Zaida Luthey-Schulten, and Peter G. Wolynes. 2004. ‘Water in Protein Structure Prediction’. *Proceedings of the National Academy of Sciences of the United States of America* 101(10):3352–57. doi: 10.1073/pnas.0307851100.
Pérez, Cristóbal, Matt Muckle, Daniel Zaleski, Nathan Seifert, Berhane Temelso, George Shields, Zbigniew Kisiel, and Brooks Pate. 2012. ‘Structures of Cage, Prism, and Book Isomers of Water Hexamer from Broadband Rotational Spectroscopy’. *Science* 336(6083):897–901. doi: 10.1126/science.1220574.
Pupo, Amaury, David Baez-Nieto, Agustín Martínez, Ramón Latorre, and Carlos González. 2014. ‘Proton Channel Models: Filling the Gap between Experimental Data and the Structural Rationale’. *Channels* 8(3):180–92.
Qiu, Feng, Santiago Rebolledo, Carlos Gonzalez, and H. Peter Larsson. 2013. ‘Subunit Interactions during Cooperative Opening of Voltage-Gated Proton Channels’. *Neuron* 77(2):288–98. doi: 10.1016/j.neuron.2012.12.021.
Ramsey, I. Scott, Younes Mokrab, Ingrid Carvacho, Zara A. Sands, Mark S. P. Sansom, and David E. Clapham. 2010. ‘An Aqueous H + Permeation Pathway in the Voltage-Gated Proton Channel Hv1’. *Nature Structural and Molecular Biology* 17(7):869–75. doi: 10.1038/nsmb.1826.
Ramsey, I. Scott, Magdalene M. Moran, Jayhong A. Chong, and David E. Clapham. 2006. ‘A Voltage-Gated Proton-Selective Channel Lacking the Pore Domain’. *Nature* 440(7088):1213–16. doi: 10.1038/nature04700.
Randolph, Aaron L., Younes Mokrab, Ashley L. Bennett, Mark SP Sansom, and Ian Scott Ramsey. 2016. ‘Proton Currents Constrain Structural Models of Voltage Sensor Activation’. doi: 10.7554/eLife.18017.001.
Rasaiah, Jayendran C., Shekhar Garde, and Gerhard Hummer. 2008. ‘Water in Nonpolar Confinement: From Nanotubes to Proteins and Beyond’. *Annual Review of Physical Chemistry* 59:713–40. doi: 10.1146/annurev.physchem.59.032607.093815.

Sakata, Souhei, Tatsuki Kurokawa, Morten H. H. Nørholm, Masahiro Takagi, Yoshifumi Okochi, Gunnar Von Heijne, and Yasushi Okamura. 2010a. 'Functionality of the Voltage-Gated Proton Channel Truncated in S4'. *Proceedings of the National Academy of Sciences of the United States of America* 107(5):2313–18. doi: 10.1073/pnas.0911868107.

Sasaki, Mari, Masahiro Takagi, and Yasushi Okamura. 2006. 'A Voltage Sensor-Domain Protein Is a Voltage-Gated Proton Channel'. *Science* 312(5773):589–92. doi: 10.1126/science.1122352.

Schladt, T. Moritz, and Thomas K. Berger. 2020. 'Voltage and PH Difference across the Membrane Control the S4 Voltage-Sensor Motion of the Hv1 Proton Channel'. *Scientific Reports* 10(1). doi: 10.1038/s41598-020-77986-z.

Schobert, Brigitte, Leonid S. Brown, and Janos K. Lanyi. 2003. 'Crystallographic Structures of the M and N Intermediates of Bacteriorhodopsin: Assembly of a Hydrogen-Bonded Chain of Water Molecules between Asp-96 and the Retinal Schiff Base'. *Journal of Molecular Biology* 330(3):553–70. doi: 10.1016/S0022-2836(03)00576-X.

Sigworth, Frederick J. 1980. 'The Variance of Sodium Current Fluctuations at the Node of Ranvier'. *The Journal of Physiology* (307):97–129.

Starace, Dorine M., Enrico Stefani, and Francisco Bezanilla. 1997. *Voltage-Dependent Proton Transport by the Voltage Sensor of the Shaker K Channel Gating Charge Movement and How It Couples to Channel Opening Requires Characterization of Both the Conforma-Tional Changes That Occur and the Local Electric Field That*. Vol. 19.

Takeshita, K., S. Sakata, E. Yamashita, Y. Fujiwara, A. Kawanabe, T. Kurokawa, Y. Okochi, M. Matsuda, H. Narita, Y. Okamura, and A. Nakagawa. 2014. 'X-Ray Crystal Structure of Voltage-Gated Proton Channel'. *Nat Struct.Mol.Biol.* 21(4):352–57. doi: 10.1038/nsmb.2783.

Tombola, Francesco, Maximilian H. Ulbrich, and Ehud Y. Isacoff. 2008. 'The Voltage-Gated Proton Channel Hv1 Has Two Pores, Each Controlled by One Voltage Sensor'. *Neuron* 58(4):546–56. doi: 10.1016/j.neuron.2008.03.026.

Tu, Yu-Hsiang, Alexander J. Cooper, Bochuan Teng, Rui B. Chang, ‡ Daniel, J. Artiga, Heather N. Turner, Eric M. Mulhall, Wenlei Ye, Andrew D. Smith, and Emily R. Liman. 2018. *An Evolutionarily Conserved Gene Family Encodes Proton-Selective Ion Channels*.

Wikström, Mårten, Michael I. Verkhovsky, and Gerhard Hummer. 2003. 'Water-Gated Mechanism of Proton Translocation by Cytochrome c Oxidase'. *Biochimica et Biophysica Acta - Bioenergetics* 1604(2):61–65. doi: 10.1016/S0005-2728(03)00041-0.

Yu, B., M. Blaber, A. M. Gronenborn, G. M. Clore, and D. L. D. Caspar. 1999. *Disordered Water within a Hydrophobic Protein Cavity Visualized by X-Ray Crystallography*. Vol. 96.

Zhang, Lejie, Karl Bellve, Kevin Fogarty, and William R. Kobertz. 2016. 'Fluorescent Visualization of Cellular Proton Fluxes'. *Cell Chemical Biology* 23(12):1449–57. doi: 10.1016/j.chembiol.2016.10.013.

Zhao, Chang, and Francesco Tombola. 2021. 'Voltage-Gated Proton Channels from Fungi Highlight Role of Peripheral Regions in Channel Activation'. *Communications Biology* 4(1):1–13. doi: 10.1038/s42003-021-01792-0.

# Articles published during the development of this doctoral thesis

Below is the list of references for the articles published by the PhD candidate during the development of this doctoral thesis, in chronological order. This list includes two research articles and three review articles.

1) **(Research article)**

Carmona, E. M., Fernandez, M., **Alvear-Arias, J. J**., Neely, A., Larsson, H. P., Alvarez, O., ... & Gonzalez, C. **(2021)**. The voltage sensor is responsible for ΔpH dependence in Hv1 channels. *Proceedings of the National Academy of Sciences*, *118*(19), e2025556118, https://doi.org/10.1073/pnas.2025556118.

2) **(Research article)**

**Alvear-Arias, J. J**., Carrillo, C., Villar, J. P., Garcia-Betancourt, R., Peña-Pichicoi, A., Fernandez, A., ... & Gonzalez, C. **(2022)**. Expression of Hv1 proton channels in myeloid-derived suppressor cells (MDSC) and its potential role in T cell regulation. *Proceedings of the National Academy of Sciences*, *119*(15), e2104453119, https://doi.org/10.1073/pnas.2104453119.

3) **(Literature Review)**

Ozu, M., **Alvear-Arias, J. J**., Fernandez, M., Caviglia, A., Peña-Pichicoi, A., Carrillo, C., ... & Gonzalez, C. **(2022)**. Aquaporin Gating: A New Twist to Unravel Permeation through Water Channels. *International Journal of Molecular Sciences*, *23*(20), 12317, http://dx.doi.org/10.3390/ijms232012317.

4) **(Literature Review)**

**Alvear-Arias, J. J**., Pena-Pichicoi, A., Carrillo, C., Fernandez, M., Gonzalez, T., Garate, J. A., & Gonzalez, C. **(2023)**. Role of Voltage-Gated Proton Channel (Hv1) in Cancer Biology. *Frontiers in Pharmacology*, *14*, 1097. doi: 10.3389/fphar.2023.1175702.

5) **(Literature Review)**

Ozu, M., Galizia, L., **Alvear-Arias, J.J**., Fernandez, M., Caviglia, A., … & Garate, J.A. **(2023)**. Mechanosensitive Aquaporins. *Biophysical Reviews*, http://dx.doi.org/10.1007/s12551-023-01098-x